Inorganic Chemistry
Cite This: Inorg. Chem. 2018, 57, 3568−3578
Forum Article
pubs.acs.org/IC

An Allosterically Regulated, Four-State Macrocycle

Andrea I. d'Aquino,[†] Ho Fung Cheng,[†] Joaquín Barroso-Flores,[‡] Zachary S. Kean,[†] Jose Mendez-Arroyo,[†] C. Michael McGuirk,[†] and Chad A. Mirkin*[,†]

[†]Department of Chemistry and International Institute for Nanotechnology, Northwestern University, 2145 Sheridan Road, Evanston, Illinois 60208, United States

[‡]Centro Conjunto de Investigación en Química Sustentable, UAEM-UNAM, Carretera Toluca-Atlacomulco Km 14.5, Personal de la UNAM, Unidad San Cayetano, Toluca, Estado de México C.P. 50200, México

Supporting Information

ABSTRACT: Macrocycles capable of host−guest chemistry are an important class of structures that have attracted considerable attention because of their utility in chemical separations, analyte sensing, signal amplification, and drug delivery. The deliberate design and synthesis of such structures are rate-limiting steps in utilizing them for such applications, and coordination-driven supramolecular chemistry has emerged as a promising tool for rapidly making large classes of such systems with attractive molecular recognition capabilities and, in certain cases, catalytic properties. A particularly promising subset of such systems are stimuli-responsive constructs made from hemilabile ligands via the weak-link approach (WLA) to supramolecular coordination chemistry. Such structures can be reversibly toggled between different shapes, sizes, and charges based upon small-molecule and elemental-anion chemical effectors. In doing so, one can deliberately change their recognition properties and both stoichiometric and catalytic chemistries, thereby providing mimics of allosteric enzymes. The vast majority of structures made to date involve two-state systems, with a select few being able to access three different states. Herein, we describe the synthesis of a new allosterically regulated four-state macrocycle assembled via the WLA. The target structure was made via the stepwise assembly of ditopic bidentate hemilabile N-heterocyclic carbene thioether (NHC,S) and phosphino thioether (P,S) ligands at Pt^{II} metal nodes. The relatively simple macrocycle displays complex dynamic behavior when addressed with small-molecule effectors, and structural switching can be achieved with several distinct molecular cues. Importantly, each state was fully characterized by multinuclear NMR spectroscopy and, in some cases, single-crystal X-ray diffraction studies and density functional theory computational models. This new structure opens the door to complex multicue switching reminiscent of multistate chemoswitches that could be important in controlling stoichiometric and catalytic transformations as well as generating molecular logic systems.

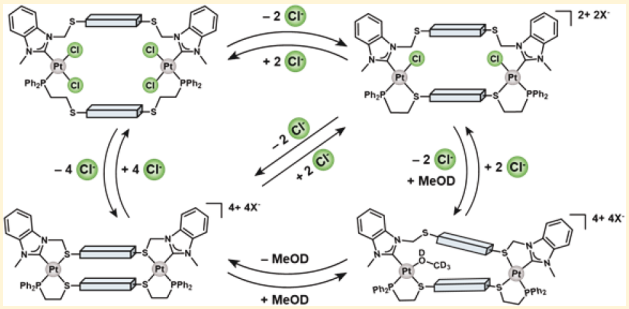

INTRODUCTION

The rational design of supramolecular systems, which undergo reversible structural changes, has been a long-standing goal of chemists because of the potential for developing technologically useful catalysts, switches, and sensors.[1,2] Coordination-driven supramolecular chemistry has emerged as a powerful means to assemble large and complex macrocycles, cages, and capsules, with general methods developed by several groups,[3−11] including our own,[12−14] for assembling such multicomponent structures. Among the different approaches to coordination-driven supramolecular constructs, the weak-link approach (WLA) has emerged as a powerful means for synthesizing complexes that can undergo reversible small-molecule-induced structural changes and therefore be toggled between "closed" rigid states and "open" flexible ones (Figure 1a−c).[10,11,15] Through the modular and convergent assembly of metal ions and hemilabile ligands, the WLA provides a platform for engineering molecular selectivity and stimuli-responsiveness with deliberate control. WLA-based supramolecular systems are attractive because they offer (1) chemical access to multiple different states with tailorable selectivity and binding affinities,[16,17] (2) high functional group tolerance,[11,18] and (3) modularity, including access to structures with a wide variety of metal nodes and ligand types.[9,10,18] Many stimuli-responsive systems have been developed based on this platform, through the incorporation of catalytic,[19−23] redox-active,[24,25] and host−guest recognition sites[17] into the ligands in such a way that small-molecule-induced structural changes result in marked changes in the properties of these complexes.

The addressable nature of these structures arises from the hemilabile phosphinoalkyl chalcoether or amine (P,X; P = $Ph_2PCH_2CH_2$− and X = O, S, Se, N) ligands typically

Special Issue: Self-Assembled Cages and Macrocycles

Received: November 1, 2017
Published: January 5, 2018

DOI: 10.1021/acs.inorgchem.7b02745
Inorg. Chem. 2018, 57, 3568−3578

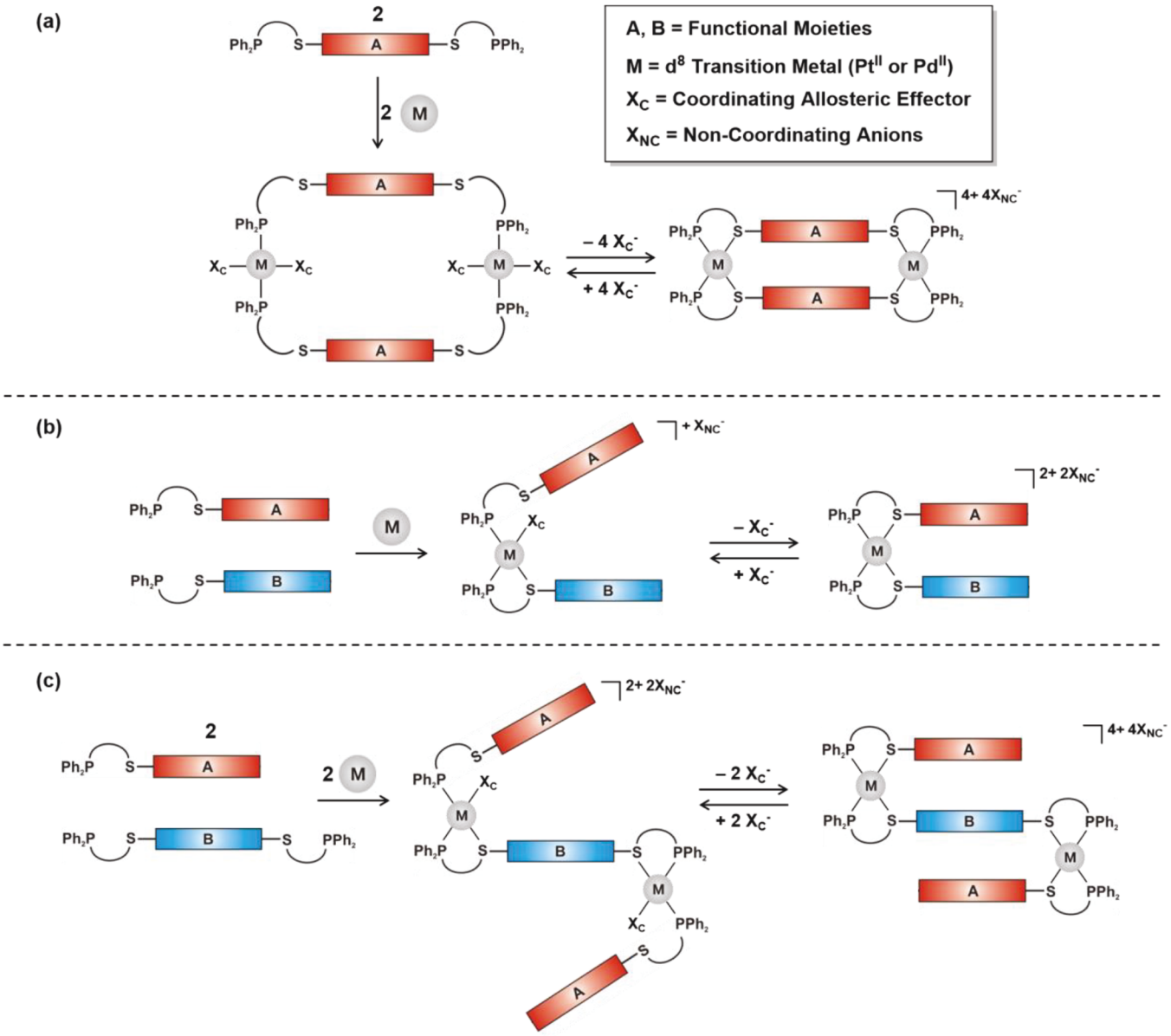

Figure 1. WLA to coordination-driven supramolecular (a) macrocycles, (b) tweezers, and (c) triple-decker complexes. For the sake of this example, complexes with Pd^{II} and Pt^{II} metal centers are illustrated, but the WLA works with many other metal systems including Rh^{I}, Cu^{I}, and Ir^{I}.[26−29]

coordinated to d^8 transition metals (such as Rh^{I}, Pd^{II}, or Pt^{II}). These complexes can reversibly access three distinct states (fully open, semiopen, and fully closed) through the removal and introduction of small molecules coordinating ligands (X_C) or elemental anions, which can easily displace the metal−S bond ("weak-link", in this example), while preserving the metal−P bond ("strong-link"; Figure 1; for simplicity, the semiopen macrocycle is not shown in Figure 1a and the fully open states are omitted from Figure 1b,c). Recently, our group reported the stepwise synthesis of heteroligated Pt^{II} WLA tweezer and triple-decker complexes with monotopic bidentate hemilabile N-heterocyclic carbene thioether (NHC,S) and phosphino thioether (P,S) ligands (Scheme 1a).[30] This strategy allowed for the assembly of air-stable heteroligated structures without the requirement of different electron-donating abilities at the "weak-links", a requisite for previous heteroligated Pt^{II} WLA systems.[31] This stepwise approach was demonstrated in the synthesis of heteroligated tweezer and triple-decker complexes.[30] Recently, this approach was used to synthesize a switchable molecular receptor that can access two distinct structural states: flexible "open" and rigid "closed" states (Scheme 1b).[16] Although this construct was the first example of a heteroligated Pt^{II} macrocyclic system, the limited structural states accessible by this complex prevented switching between multiple binding pockets, each capable of binding a different guest molecule or exhibiting a different, but complementary function. Developing allosterically regulated structures that can access multiple states with different properties is a fundamental challenge and remains an important synthetic goal. The structures reported herein are the first step toward the development of multistate, stimuli-responsive receptors, catalysts, and chemoswitches, with fundamentally interesting functions relating to their different chemically tunable structures.

Herein, we apply this stepwise approach to the synthesis of a heteroligated multistate macrocycle, possessing two different

DOI: 10.1021/acs.inorgchem.7b02745
Inorg. Chem. 2018, 57, 3568−3578

Scheme 1. (a) Stepwise Approach to the Synthesis of WLA Tweezer and Triple-Decker Complexes, (b) Stepwise Assembly of a WLA Heteroligated Pt^{II} Macrocyclic Capsule, and (c) the Scope of This Work Applying This Approach to the Synthesis of an Allosterically Regulated, Multistate, Heteroligated Macrocycle[a]

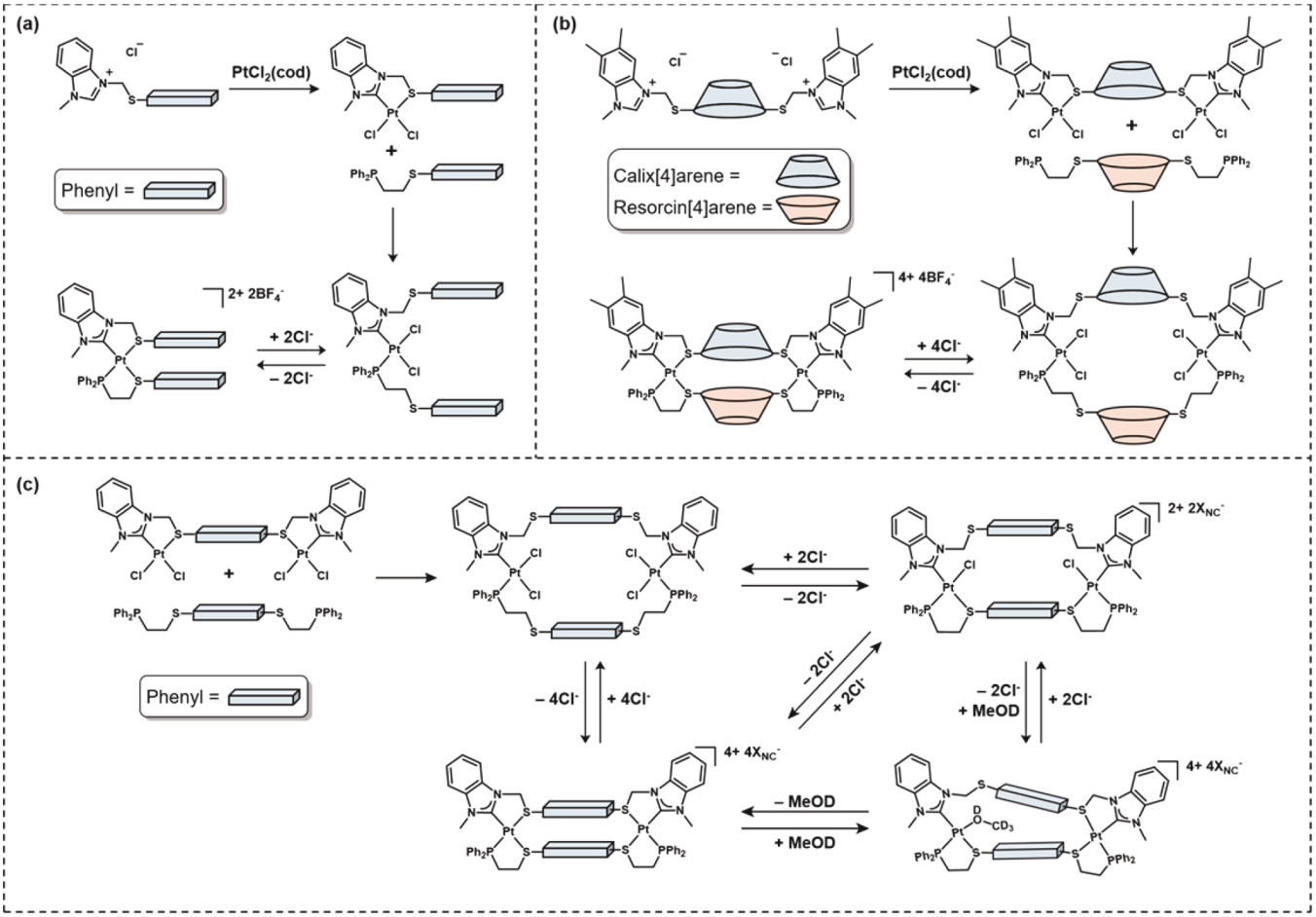

[a]MeOD = methanol-d_4.

ditopic bidentate ligands bridging two Pt^{II} metal nodes, which exhibits four-state switching behavior, considerably more complex than previously reported for WLA systems (Scheme 1c). Experimental and computational evidence suggest that, while the addressability of the system arises from the coordination chemistry, the resulting complexity of the macrocycle behavior is a function of multiple factors, including geometry, strain, strength of coordination bonds, and electronics. This is in contrast with previously reported WLA systems that rely on the use of weakly chelating ligands to achieve the assembly of heteroligated structures, which are too unstable to form significantly strained structures.[11]

RESULTS AND DISCUSSION

WLA Macrocycle Synthesis and Characterization. In order to synthesize the Pt^{II} heteroligated WLA macrocycle, we utilized a previously reported stepwise approach employing a ditopic bidentate NHC,S-based ligand in conjunction with a traditional ditopic bidentate P,S-based ligand, both of which bind Pt^{II} strongly enough to result in kinetically stable structures. Benzimidazolium chloride salt **1** was treated with 2 equiv of dichloro(1,5-cyclooctadiene)platinum(II) [$PtCl_2$(cod)] and 1 equiv of silver(I) oxide (Ag_2O) in dichloromethane (CH_2Cl_2) to produce $Pt_2Cl_4(\kappa^2{:}\mu{:}\kappa^2$-NHC,S) (**2**) as an insoluble white solid (Scheme 2). In order to confirm that the metalation reaction of **1** with Ag_2O and the subsequent transmetalation reaction with $PtCl_2$(cod) were successful, complex **2** was characterized by matrix-assisted laser desorption/ionization time-of-flight mass spectrometry (MALDI-TOF MS), with the monoisotopic mass and isotopic distribution matching those of the molecular ion $[M - Cl]^+$ (see the Supporting Information, SI). Because of the low solubility of complex **2** in CH_2Cl_2, single crystals suitable for X-ray diffraction were obtained by the slow diffusion of diethyl ether (Et_2O) into a solution of complex **2** in dimethyl sulfoxide (DMSO). The solid-state structure reveals a complex with DMSO ligands coordinated to the metal center, displacing the weakly bound thioether groups on the NHC,S hemilabile ligand (see the SI).

The irreversible metalation–transmetalation reaction at the NHC ligand allows for the subsequent use of strongly binding P,S ligands without the occurrence of previously observed ligand-exchange reactions.[31,32] Because of the low solubility of **2** in CH_2Cl_2, complex **2** was dissolved in a 1:1 mixture of CH_2Cl_2 and methanol (MeOH) and reacted with 1 equiv of the P,S-aryl-S,P ligand **3** (Scheme 2). Characterization of the resulting product by ^1H and ^{31}P NMR spectroscopy revealed that the fully open macrocycle was obtained as a mixture of isomers (**4a–4c**) when synthesized under homogeneous conditions in a 1:1 mixture of MeOH and CH_2Cl_2 (Scheme

DOI: 10.1021/acs.inorgchem.7b02745
Inorg. Chem. 2018, 57, 3568–3578

Scheme 2. Synthesis of Fully Open Heteroligated Macrocycles 4a–4c[a]

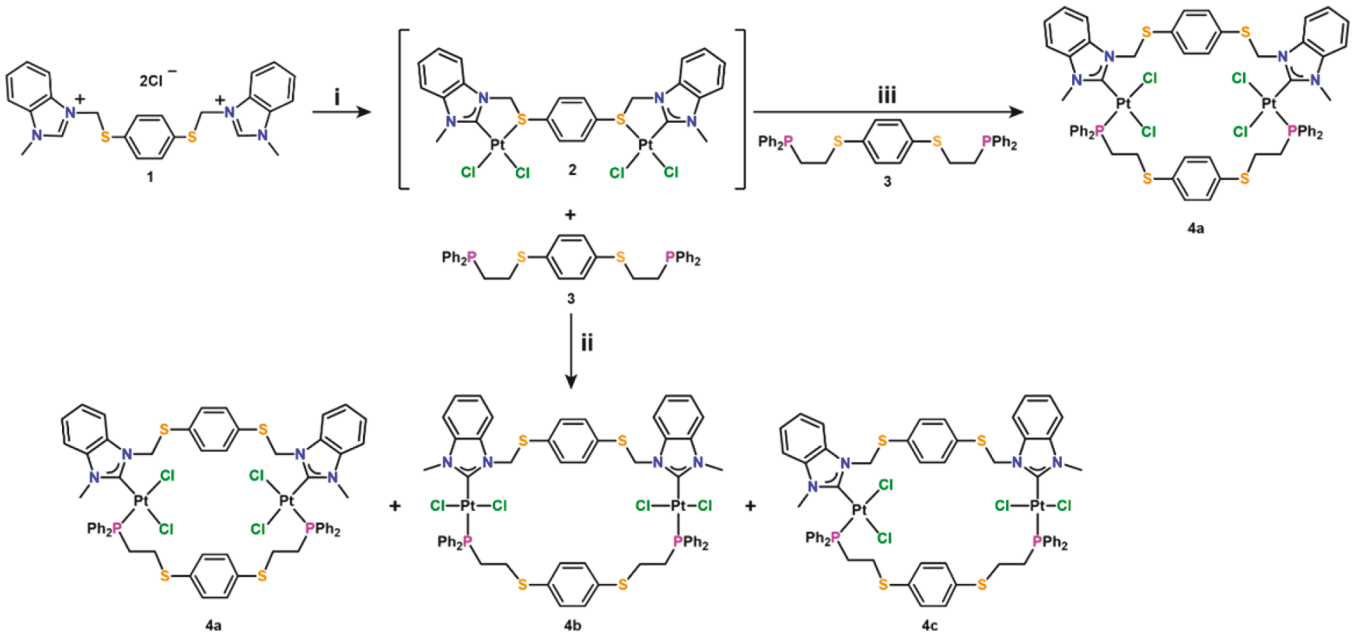

[a]Reaction conditions: (i) 2 equiv of $PtCl_2(cod)$; 1 equiv of Ag_2O; 6:1 CH_2Cl_2/MeOH, 24 h, 60 °C. (ii) 1:1 MeOH/CH_2Cl_2, 25 °C. (iii) CH_2Cl_2, 25 °C.

2). Consistent with this observation, a high-resolution mass spectrometry (HRMS) spectrum of the sample exhibited a peak with a mass-to-charge (m/z) ratio corresponding to the molecular ion $[M - Cl]^+$ (see the SI).

^{31}P NMR spectroscopy was used to further characterize the resulting compounds because it is highly diagnostic of the coordination environment. Additionally, the resonance shifts and platinum–phosphorus coupling patterns were consistent with the presence of a combination of *cis*-**4a**, *trans*-**4b**, and combined cis/trans (**4c**) fully open complexes (Figure 2a).[33−35] As summarized in Figure 2, the fully open trans species **4b** [*trans*-$Pt_2Cl_4(\kappa^1{:}\mu{:}\kappa^1$-NHC,S)$(\kappa^1{:}\mu{:}\kappa^1$-P,S)] contains two platinum nodes in which the phosphine and carbene are trans to one another; this configuration is evidenced by a resonance at 9.7 ppm with a J_{P-Pt} coupling constant of 2300 Hz. The presence of the cis complex **4a** [*cis*-$Pt_2Cl_4(\kappa^1{:}\mu{:}\kappa^1$-NHC,S)-$(\kappa^1{:}\mu{:}\kappa^1$-P,S)] is evidenced by a resonance at 1.8 ppm with a larger J_{P-Pt} of 3740 Hz. Downfield from each of the two major resonances are additional sets of signals at 2.5 and 10.5 ppm, which are of equal intensity relative to one another (Figure 2a). We proposed that they correspond to a species that has both cis and trans nodes in one complex, **4c** [*cis*-$PtCl_2(\kappa^1{:}\mu{:}\kappa^1$-NHC,S)$(\kappa^1{:}\mu{:}\kappa^1$-P,S)-*trans*-$PtCl_2(\kappa^1{:}\mu{:}\kappa^1$-NHC,S)$(\kappa^1{:}\mu{:}\kappa^1$-P,S)]. This assignment is supported by the $^{31}P-^{195}Pt$ coupling constants, which are comparable to that of the purely cis and purely trans isomers (Figure 2). The relative chemical shifts along with the $^{31}P-^{195}Pt$ coupling constants reveal important information about the trans influence inherent to these structures.[34−36] In the case of strongly donating ligands, the chemical shift typically appears further downfield,[35] such as in the trans complex **4b**. Between isostructural complexes, larger $^{31}P-^{195}Pt$ coupling constants are indicative of a more weakly coordinating ligand trans to the phosphine ligand, while smaller coupling constants indicate the presence of a more strongly coordinating ligand. The NHC is a more strongly donating ligand than the chloride; therefore, the coupling constant of the

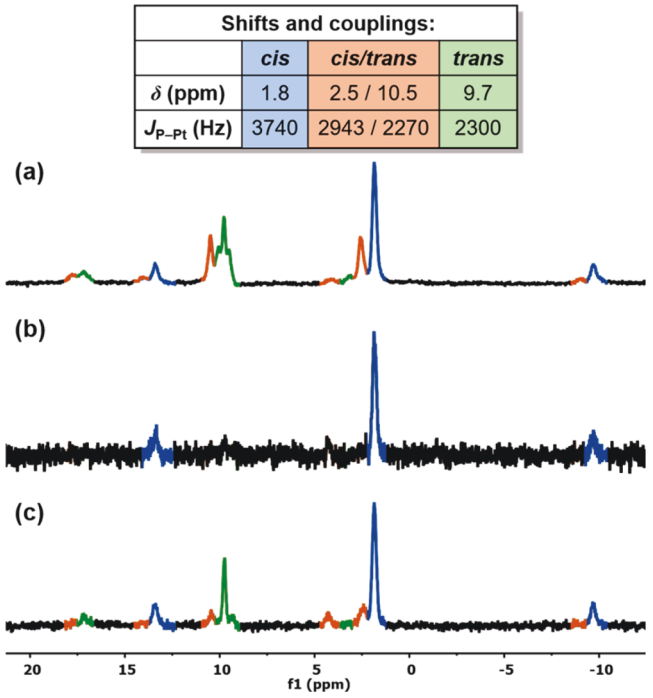

Figure 2. (a) ^{31}P NMR spectrum of the complex mixture **4** in CD_2Cl_2, (b) ^{31}P NMR spectrum of single crystals of the fully open cis complex **4a** dissolved in CD_2Cl_2, (c) ^{31}P NMR spectrum of **4a** after several hours, indicating the reappearance of resonances attributable to the cis (**4a**), trans (**4b**), and cis/trans (**4c**) species.

trans complex **4b** (J_{P-Pt} = 2300 Hz) is significantly smaller than that of the cis complex **4a** (J_{P-Pt} = 3740 Hz). The cis/trans species (**4c**) follows the same trend, with one Pt^{II} node in the cis configuration and the other in the trans orientation, each having a chemical shift and coupling constant in the same region of the spectrum as the fully cis and trans counterparts,

DOI: 10.1021/acs.inorgchem.7b02745
Inorg. Chem. 2018, 57, 3568−3578

respectively. The resonance at 2.5 ppm has a larger coupling constant (J_{P-Pt} = 2943 Hz), while the resonance of equal intensity further downfield at 10.5 ppm has a smaller coupling constant (J_{P-Pt} = 2270 Hz).

When the solvent from the solution of **4a**–**4c** was slowly evaporated, single crystals composed exclusively of **4a** were isolated. The solid-state structure of **4a** is consistent with the solution-phase spectroscopic characterization of the fully open cis isomer, with one κ^1:μ:κ^1-P,S ligand and one κ^1:μ:κ^1-NHC,S ligand coordinated to Pt^{II} through the phosphines and carbenes, respectively (Figure 3). We hypothesized that the

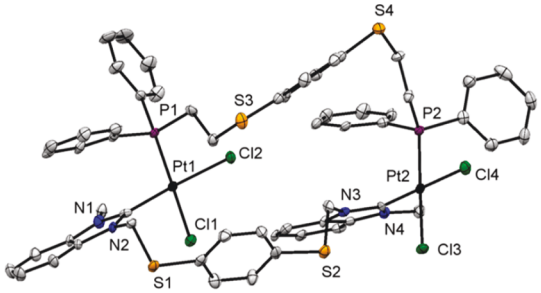

Figure 3. Crystal structure of **4a**, drawn with a 50% thermal ellipsoid probability. Solvent molecules and H atoms have been omitted for clarity. Selected bond lengths [Å] and angles [deg]: Pt1–Cl2 2.360(2), Pt1–Cl2 2.352(2), Pt2–Cl3 2.340(2), Pt2–Cl4 2.357(2); Cl1–Pt1–Cl2 90.57(6), Cl3–Pt2–Cl4 89.42(6).

fully open cis structure would dynamically equilibrate back to the **4a**–**4c** complexes initially observed in solution, an indication of fully open isomers that are similar in energy. To assess the kinetic stability of **4a**, its crystals were dissolved in CD_2Cl_2 and the corresponding ^{31}P NMR spectrum was collected (Figure 2b), confirming our assignment of the 1.8 ppm shift belonging to **4a**. Over time, we observed the reappearance of resonances attributable to the trans (**4b**) and cis/trans (**4c**) species, in addition to the cis complex **4a**, indicating that the complex undergoes isomerization in solution (Figure 2c). Consistent with an equilibrium that involves small energetic differences between isomers, we observed strong solvent effects in the synthesis of **4a**–**4c**. In an alternative procedure, we reacted **2** with **3** in CH_2Cl_2 under heterogeneous conditions (Scheme 2), resulting in the selective formation of **4a**, as confirmed by ^1H and ^{31}P NMR spectroscopy and HRMS. These results suggest that solvent effects play a key role in lowering the kinetic barriers to establish an equilibrium between isomers **4a**–**4c**.

Solid-State Structure of 4a. The solid-state structure of **4a** confirms that the fully open cis complex contains two inner-sphere Cl atoms in the cis orientation. Complex **4a** crystallized in the triclinic centrosymmetric space group $P\bar{1}$, and the asymmetric unit contains distinct Pt–Cl bond lengths and angles (Figure 3) comparable to those found in the literature.[11,30] The Pt^{II} metal nodes adopt a square-planar geometry [Cl1–Pt1–Cl2 = 90.57(6)°], with the phosphine moieties cis to the carbene moieties [P1–Pt1–C1 = 94.6(2)°] (Figure 3). The solid-state structure supports the assignments made in the ^1H and ^{31}P NMR spectra (see the SI).

Computational Studies of Complexes 4a–4c. In order to further investigate and understand the intramolecular interactions and relative energies of each fully open isomer in solution, we explored the electronic structures of **4a**–**4c** and their possible diastereomers with density functional theory (DFT) calculations in the gas phase. DFT calculations were carried out on the solid-state structure of **4a** with the *Gaussian 09* suite of programs at the B97D/LANL2DZ level of theory. The selected functional B97D empirically includes dispersion effects, which allows for a better description of the electronic structure. The geometry-optimized model of **4a** provided the basis for developing the energy-minimized models of **4b** and **4c** and their respective isomers. The bond lengths and angles of model **4a** are nearly identical with those measured in the solid-state crystal structure. All structures correspond to local minima on the potential energy surfaces and, therefore, are chemically accessible states. Population analysis was performed within the natural bond orbital formalism to provide a localized, pairwise description of the electron density.

We hypothesized that complexes **4a**–**4c** would be relatively close in their free energies because of the observation of rapid and dynamic conversion from the purely cis state to the mixture of cis, trans, and cis/trans states. Energy-minimized models (Figure 4) were obtained for each complex (**4a**–**4c**), and their

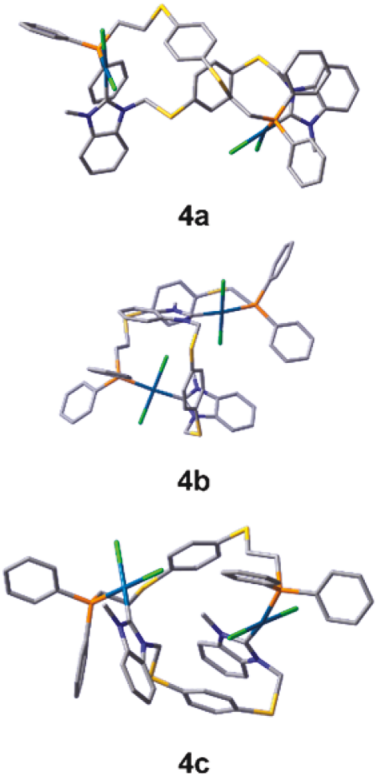

Figure 4. Energy-minimized models of complexes **4a**–**4c**, obtained from DFT calculations.

respective frontier orbitals were identified because they point to the identity of the orbitals involved in WLA bonding. The relative highest occupied molecular orbital (HOMO) and lowest unoccupied molecular orbital (LUMO) energies were calculated, and free energies were compared across different structures. Table 1 summarizes the free energies calculated from the DFT results.

Computational modeling of the fully open states suggests that the overall free energies of the three states are close enough that there is no strong preference to form one isomer over the others. This is consistent with a system that has very small energy differences between isomers, suggesting that **4a**–**4c** are nearly isoenergetic.

DOI: 10.1021/acs.inorgchem.7b02745
Inorg. Chem. 2018, 57, 3568–3578

Table 1. Free Energies (kcal/mol) of 4a–4c Obtained from DFT Calculations

compound	free energy (kcal/mol)	relative free energy (kcal/mol)
4a	−2811.3087	0.0
4b	−2811.3029	0.006
4c	−2811.3018	0.007

Formation of the Semiopen WLA Macrocycle. Upon exposure of the neutral, fully open state **4a** (or the mixture of **4a–4c**) to MeOH, the dicationic, semiopen complex [*cis*-$Pt_2Cl_2(\kappa^1{:}\mu{:}\kappa^1$-NHC,S$)(\kappa^2{:}\mu{:}\kappa^2$-P,S$)][Cl]_2$ (**5**) was formed via the transfer of a chloride anion from the inner coordination sphere of each Pt^{II} center to the outer coordination sphere (Scheme 3). In polar protic solvents such as MeOH, outer-sphere chloride counterions are stabilized by hydrogen bonding, and the overall charge of the complex is stabilized by the polar solvent, thus favoring the semiopen state. This transformation is enthalpically driven and has been observed in similar systems.[11,37,38]

The driving force of the switching from the fully open to the semiopen state is 2-fold: (i) the two outer-sphere Cl ions and the charged complex are stabilized by the polar solvent and (ii) the structure is able to relieve ring strain by adopting the semiopen configuration, as evidenced by DFT calculations (see the SI). Complex **5** was thoroughly characterized via ^{1}H and ^{31}P NMR spectroscopy, diffusion ordered spectroscopy (DOSY), two-dimensional correlation spectroscopy, and HRMS (see the SI). The chemical shift observed in the ^{31}P NMR spectrum of complex **5** (δ 36 ppm) is shifted dramatically downfield from that of the fully open Pt^{II} complexes with a concurrent decrease in the coupling constant (J_{P-Pt} = 3421 Hz; Figure 5a). The downfield chemical shift and the decrease in J_{P-Pt} are consistent with increased back-donation from the Pt atoms in the semiopen state in which the P,S ligand is fully chelated with the phosphine moiety trans to the chloride. Additionally, this downfield shift is diagnostic of phosphine-containing ligands forming a five-membered ring.[39]

A small shoulder at 37 ppm, hypothesized to be due to the presence of diastereomers, is present just downfield of the major resonance at 36 ppm in the ^{31}P NMR spectrum. Previous reports have shown that stereoisomers in WLA tweezer complexes with two phosphinoalkyl thioether ligands, as well as in WLA complexes bearing NHC,S and P,S ligands, can be observed via ^{1}H and ^{31}P NMR spectroscopy.[11,30] This is attributed to the intramolecular inversion of the thioether moiety trans to a ligand with a strong trans effect (such as phosphines).[40,41] A variable-temperature (VT) ^{31}P NMR study revealed that the two signals (36 and 37 ppm) present at room temperature coalesce at high temperature (330 K) in methanol-d_4, indicating rapid interconversion of the diastereomers in solution (Figure 6). These results were further supported by energy-minimized DFT calculations of the two diastereomers (see the SI).

Formation of a New WLA Intermediate State. The semiopen complex **5** was then reacted with 4 equiv of silver tetrafluoroborate ($AgBF_4$) in MeOH to abstract the four Cl ions (two inner sphere and two outer sphere) and form the fully closed complex with fully chelated ditopic bidentate P,S and NHC,S ligands (Scheme 4a). Despite being a widely reported method for closing WLA complexes, the reaction did not result in a fully closed complex, as evidenced by ^{31}P NMR and MALDI-TOF MS. Instead, the signals in the ^{31}P NMR spectrum indicate a seemingly nonsymmetric product, displaying two distinct ^{31}P resonances of equal intensity: one at 37 ppm and the other at 47 ppm (Figures 5a, **6**). The signal at 37 ppm is consistent with previously reported Pt^{II} semiopen complexes bearing NHC,S ligands,[30] while the resonance downfield at 47 ppm is characteristic of a fully closed complex.[30] Given that the peaks were of approximately equal intensity, we hypothesized that a new WLA structural state was obtained, namely, a macrocycle with one Pt^{II} metal center in a fully closed state and the other in a semiopen state with methanol-d_4 bound to the Pt center rather than the expected thioether moiety ([*cis*-$Pt_2(\kappa^1{:}\mu{:}\kappa^2$-NHC,S$)(\kappa^2{:}\mu{:}\kappa^2$-P,S$)$-$CD_3OD][BF_4]_4$ (**6**); Scheme 4a). This hypothesis was supported by the observation that the relative intensities of the two peaks did not change when additional $AgBF_4$ was added, indicating that the reaction had gone to completion and that the signal at 37 ppm does not belong to the residual starting material. Although single crystals suitable for X-ray diffraction were not obtained, ^{1}H and ^{31}P NMR spectroscopy, MALDI-TOF MS, and DFT calculations support the formation of complex **6**. MALDI-TOF MS analysis of complex **6** revealed a peak at m/z 1767.308, which matches the simulated mass of the molecular ion $[M + H]^+$ (see the SI). Additionally, DFT calculations were used to calculate the strength of the Pt^{II}–$OHCH_3$ bond, for comparison to the traditional Pt^{II}–S bond. The Pt^{II}–$OHCH_3$ interaction was calculated to be 30.70 kcal/mol, which is comparable to that of the Pt^{II}–S bond energy in the same compound (42.25, 57.10, and 63.77 kcal/mol), further supporting the formation of **6** (see the SI).

Scheme 3. Formation of the Semiopen WLA Macrocycle[a]

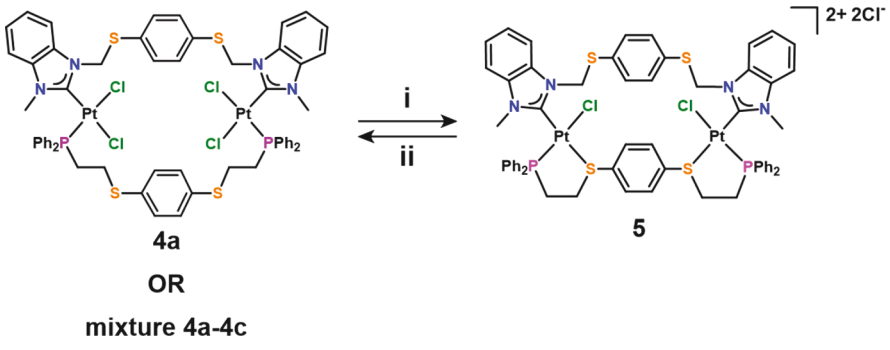

[a]Reaction conditions: (i) MeOH, 25 °C. (ii) CH_2Cl_2, 25 °C.

DOI: 10.1021/acs.inorgchem.7b02745
Inorg. Chem. 2018, 57, 3568–3578

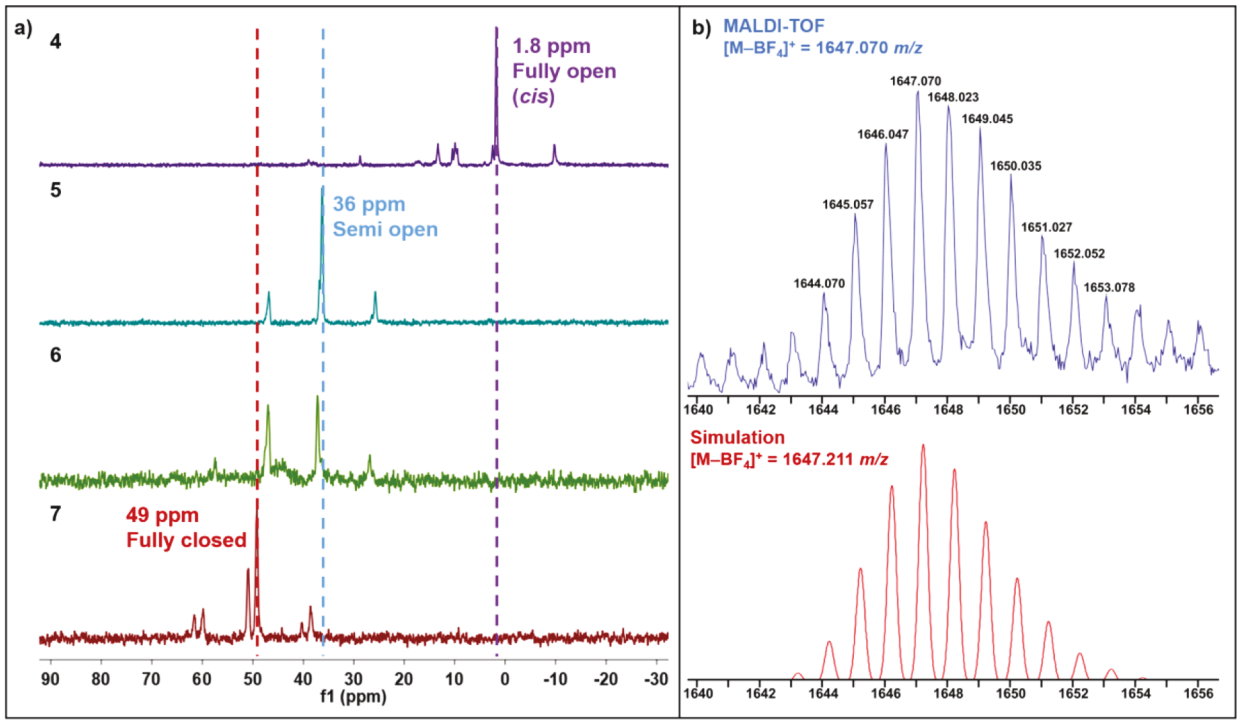

Figure 5. (a) ^{31}P NMR spectra of each distinct state accessible by the WLA macrocycle, namely, fully open (**4**), semiopen (**5**), and new intermediate (**6**) states with one Pt^{II} node in the closed state and the other in a semiopen state and a fully closed state (**7**). (b) MALDI-TOF spectrum compared with the ISOPRO simulation of the molecular ion $[M - BF_4]^+$ of complex **7**.

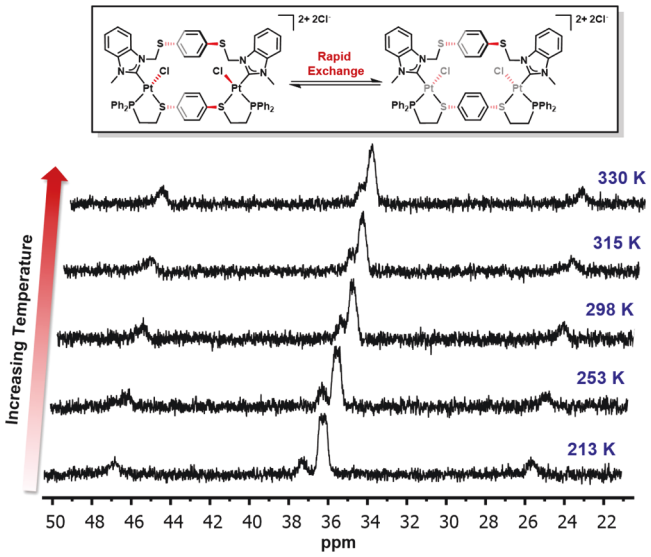

Figure 6. ^{31}P NMR spectra of complex **5** in methanol-d_4 from 213 to 330 K. Coalescence of the major resonance (36 ppm) and the corresponding diastereomer's resonance (37 ppm) is observed at high temperature, consistent with the presence of rapidly interconverting diastereomers at elevated temperature.

Formation of the Fully Closed State. In order to fully close the macrocycle, complex **6** was subjected to high vacuum for 2 h to liberate what was hypothesized to be a methanol-d_4 molecule bound to the Pt^{II} metal center and form the κ^2:μ:κ^2-NHC,S and κ^2:μ:κ^2-P,S coordinated complex (Scheme 4b). Characterization by ^{1}H and ^{31}P NMR spectroscopy (Figure 5a, **7**), MALDI-TOF MS, and DFT calculations confirmed the formation of a fully closed state. Specifically, when the fully dried product was dissolved in a noncoordinating deuterated solvent (nitromethane-d_3) and analyzed by ^{31}P NMR spectroscopy (Figure 5a, **7**), two major resonances at 49 ppm (J_{P-Pt} = 3450 Hz) and 51 ppm (J_{P-Pt} = 3450 Hz) were observed with an integral ratio of 2:1 (see the SI). This result is consistent with the formation of the fully closed complex **7** with a 2:1 mixture of diastereomers, as was the case in the semiopen complex. Complex **7** was further investigated by a VT ^{31}P NMR study from room temperature to 338 K, a temperature range in which thioether inversion was previously observed (see the SI).[30,37] The coalescence of the two signals at high temperature confirmed that the two peaks stem from the two diastereomers of the fully closed complex **7**.

To further investigate the structures and energies of the two diastereomers, energy-minimized models were calculated by DFT, and their relative energies were obtained (see the SI). The energy-minimized models suggest that both diastereomers are structurally accessible states and are comparable in their free energies, consistent with the nearly equal proportion observed in the ^{31}P NMR spectrum (see the SI). The presence of complex **7** was further confirmed by MALDI-TOF MS with a peak at m/z 1647.070, which matches the simulated isotopic distribution of the molecular ion $[M - BF_4]^+$ (Figure 5b). Additionally, complex **7** can also be obtained directly from the semiopen complex **5** via a reaction with 4 equiv of $AgBF_4$ in the noncoordinating solvent nitromethane (Scheme 4b).

Accessing Each of the Reversible States. As previously mentioned, WLA complexes are unique in their ability to be allosterically regulated in a reversible manner. As such, we sought to reopen complex **7** and reform each of the previously accessed states (Scheme 5). Complex **6** was readily regenerated from complex **7** by dissolution in MeOH. Upon the addition of 4 equiv of a soluble chloride source, namely, bis(triphenylphosphoranylidene)ammonium chloride (PPNCl), complex **6** was converted to the semiopen complex **5**. The

DOI: 10.1021/acs.inorgchem.7b02745
Inorg. Chem. 2018, 57, 3568−3578

Scheme 4. Formation of (a) the New Intermediate WLA Macrocycle State (6) and (b) the Fully Closed Macrocycle[a]

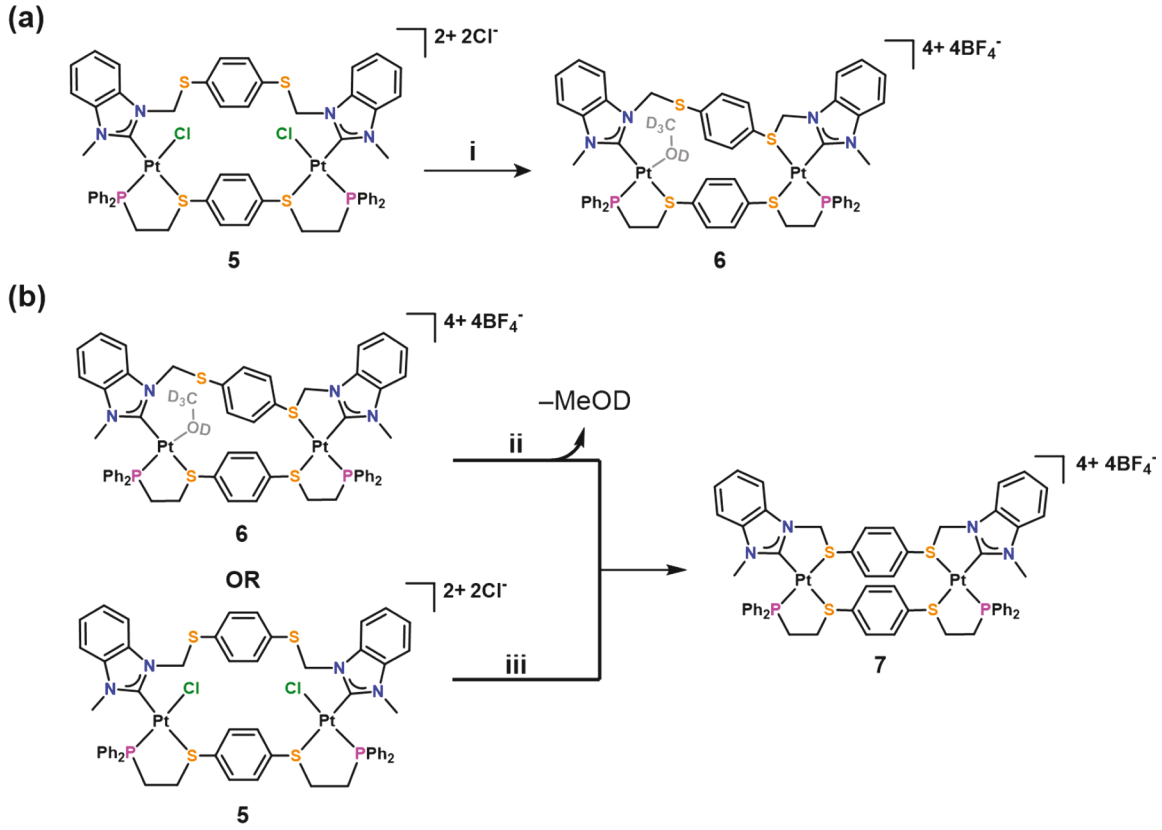

[a]Reaction conditions: (i) 4 equiv of $AgBF_4$, methanol-d_4. (ii) (1) High vacuum to remove methanol-d_4 (MeOD), 2 h; (2) CH_3NO_2-d_3. (iii) 4 equiv of $AgBF_4$, CH_3NO_2-d_3.

Scheme 5. Reversible Closing and Reopening of the WLA Multistate Macrocycle[a]

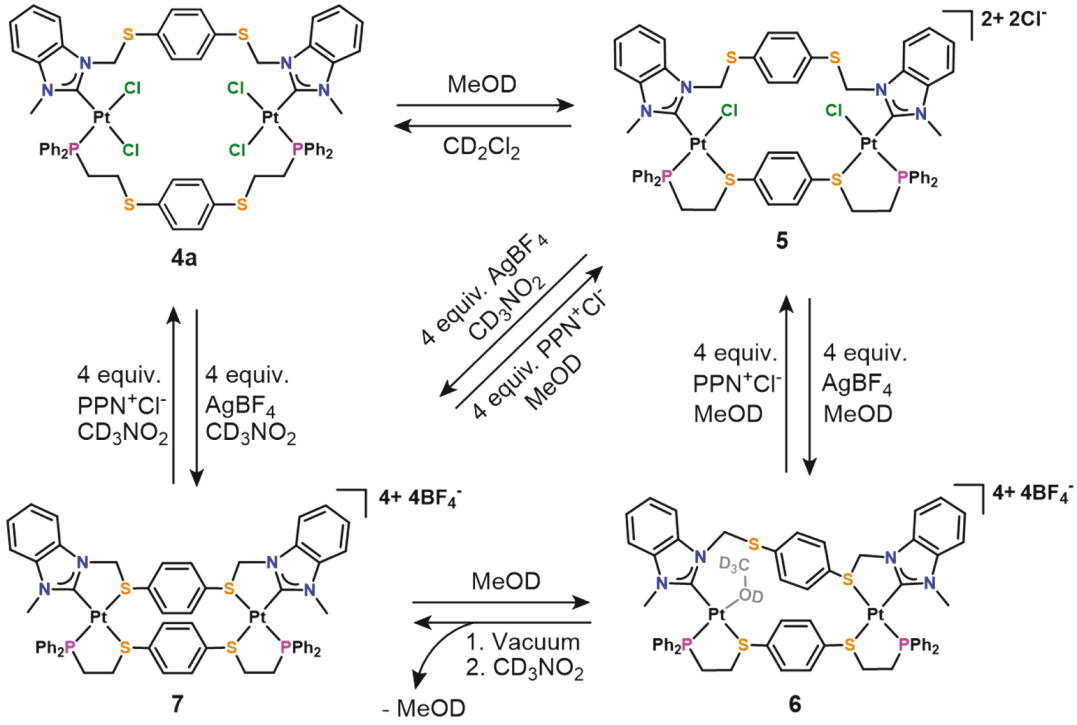

[a]MeOD = methanol-d_4.

DOI: 10.1021/acs.inorgchem.7b02745
Inorg. Chem. 2018, 57, 3568−3578

opening was evidenced by the disappearance of the signal at 47 ppm and the concomitant appearance of signals at 36 and 37 ppm, corresponding to the two diastereomers of complex **5** (see the SI). Upon dissolution of the fully dried complex **5** in CD_2Cl_2, the fully open complex **4a** was regenerated, completing the closing and reopening cycle. The ^{31}P NMR spectrum of the resulting product shows the disappearance of the resonances at 36 and 37 ppm and the reappearance of the signal at 1.8 ppm (J_{P-Pt} = 3740 Hz), consistent with the formation of the cis complex **4a** (see the SI).

CONCLUSIONS

Of the various supramolecular architectures that have been synthesized through coordination-driven supramolecular assembly, the macrocycle continues to be an important architecture because of its defined cavity, making it useful for host–guest chemistry, designed molecular recognition, and catalysis.[2] Additionally, macrocyclic architectures have paved the way for the synthesis of larger, more sophisticated structures with three-dimensional cavities. The addressable construct described here is a potentially useful building block for the construction of higher order, chemically addressable complexes with multistate switching capabilities. Key to the success of the stepwise formation of heteroligated WLA macrocycles is the kinetic stability of the complexes where the "weak-link" thioether is a relatively strong donor. The consequence of this strong bonding is illustrated by the formation of the semiopen/fully closed complex **6**, in which a MeOH molecule occupies one of the empty coordination sites. The MeOH molecule displaces a single thioether and alleviates some of the fully closed structure's strain energy, which has been investigated by DFT calculations. The ring strain present in this system suggests that the WLA may allow us to design systems in which strain can be exploited to enable the use of allosteric effectors that are not anionic. The result is a macrocyclic structure that can adopt new intermediate states previously not observed in traditional WLA systems, making it the first platinum-based system to require multiple cues or stimuli to be switched between states and the only known four-state WLA system.

EXPERIMENTAL SECTION

General Methods/Instrument Details. Commercially available chemicals were purchased as reagent grade from Sigma-Aldrich, Acros, and Alfa Aesar, unless otherwise noted, and used as received. Unless otherwise stated, all solvents were purchased anhydrous and degassed under a stream of argon prior to use. All glassware and magnetic stirring bars were thoroughly dried in an oven (180 °C). Reactions were monitored using thin-layer chromatography (TLC), commercial TLC plates (silica gel 254, Merck Co.) were developed, and the spots were visualized under UV light at 254 or 365 nm. Flash chromatography was performed using SiO_2-60 (230–400 mesh ASTM, 0.040–0.063 mm; Fluka). Deuterated solvents were purchased from Cambridge Isotope Laboratories and used as received. ^1H, ^{31}P, $^{31}P\{^1H\}$, and $^{19}F\{^1H\}$ NMR spectra were recorded on a Bruker Avance 400 MHz spectrometer, and chemical shifts (δ) are given in parts per million. ^1H NMR spectra were referenced internally to residual proton resonances in the deuterated solvents (dichloromethane-d_2 = δ 5.32; nitromethane-d_3 = δ 4.33; methanol-d_4 = δ 3.31). ^{31}P and $^{31}P\{^1H\}$ NMR spectra were referenced to an external 85% H_3PO_4 standard (δ 0). High-resolution mass spectrometry (HRMS) measurements were recorded on an Agilent 6120 LC-TOF instrument in positive-ion mode. Electrospray ionization mass spectrometry (ESI-MS) was recorded on a Micromas Quatro II triple–quadrapole mass spectrometer. Matrix-assisted laser desorption/ionization time-of-flight mass spectrometry (MALDI-TOF MS) was recorded on a Bruker Autoflex III smartbeam in reflectron and positive-ion mode.

Synthesis. *Benzimidazolium Salt (**1**).* In a modified procedure,[30] a solution of 1,4-bis[(chloromethyl)thio]benzene (50 mg, 0.209 mmol) and 1-methylbenzimidazole (74.09 mg, 0.627 mmol) was dissolved in 5 mL of anhydrous dimethylformamide. The reaction mixture was stirred and heated at 100 °C for 24 h in a Schlenk flask under N_2 gas. The solvent was reduced to ca. 1 mL in vacuo with heptane. The product was then washed with diethyl ether (Et_2O) and dichloromethane (CH_2Cl_2) and dried in vacuo to obtain a white solid (66.3 mg, 0.132 mmol, 63% yield). ^1H NMR (400 MHz, DMSO-d_6): δ 9.85 (s, 2H), 7.68 (dtd, J = 15.7, 7.4, and 6.3 Hz, 4H), 7.72–7.64 (m, 4H), 7.37 (s, 4H), 6.17 (s, 4H), 4.05 (s, 6H). ^{13}C NMR (126 MHz, DMSO-d_6): δ 142.32, 132.31, 131.98, 131.67, 130.12, 126.79, 126.67, 114.06, 113.91, 49.83, 33.42.

[$Pt_2Cl_4(\kappa^1{:}\mu{:}\kappa^1$-NHC,S)$(C_2H_6OS)_2$] (2-DMSO). A solution of benzimidazolium salt (**1**) (100 mg, 0.199 mmol) in a solvent mixture of CH_2Cl_2/MeOH at a ratio of 6:1 (4 mL) was combined with Ag_2O (46 mg, 0.199 mmol), and the mixture was stirred at 60 °C until the solution became murky and the black Ag_2O powder disappeared. After 10 min, a solution of $PtCl_2$(cod) (149 mg, 0.397 mmol) in the solvent mixture of CH_2Cl_2/MeOH at a ratio of 6:1 (6 mL) was added to the mixture, which was then stirred at 60 °C over 24 h. The suspension was centrifuged, washed with Et_2O (10 mL × 3), and dried in vacuo. The product was obtained as an off-white powder (115 mg, 0.120 mmol, 60% yield). ^1H NMR (400 MHz, DMSO-d_6): δ 7.74 (dd, J = 8.2 and 3.7 Hz, 2H), 7.41 (d, J = 1.7 Hz, 4H), 7.35 (t, J = 7.7 Hz, 2H), 7.29–7.16 (m, 4H), 6.20–6.02 (m, 4H), 4.19 (d, J = 3.6 Hz, 6H). ^{13}C NMR (126 MHz, DMSO-d_6): δ 155.68 (d, $^1J_{C-Pt}$ = 4.2 Hz), 133.17 (s), 133.05 (s), 132.73 (s), 132.66 (s), 124.02 (s), 123.89 (s), 111.69 (s), 111.36 (s), 111.31 (s), 51.37 (s), 34.83 (s). MALDI-TOF MS (matrix: dithranol). Calcd for $[M - Cl]^+$: m/z 926.961. Found: m/z 926.803.

*1,4-Bis(diphenylphosphino)ethylthiobenzene (**3**).* In a modified procedure,[42,43] benzene-1,4-dithiol (0.340 mg, 2.36 mmol) was combined with azobis(isobutyronitrile) (catalytic amount) in a Schlenk flask in THF (15 mL) under N_2 gas. Diphenylvinylphosphine ($KPPh_2$; 1.0 g, 4.71 mmol) was added dropwise to the reaction mixture, via a syringe, under N_2 gas over the course of 30 min. The solution turned from yellow to red. The reaction was refluxed for 18 h under N_2 gas. After stirring for 18 h, the reaction solution was concentrated in vacuo to give a yellow oil. The crude product was washed with hexanes (10 mL × 3) followed by MeOH (10 mL × 3), filtered, and dried under high vacuum. The pure product appeared as an off-white solid powder (1.18 g, 90% yield). ^1H NMR (400 MHz, CD_2Cl_2): δ 7.41–7.35 (m, 8H), 7.34–7.31 (m, 12H), 7.10 (s, 4H), 2.96–2.90 (m, 4H), 2.36–2.32 (m, 4H). ^{31}P NMR (162 MHz, CD_2Cl_2): δ −17.36.

*[cis-$Pt_2Cl_4(\kappa^1{:}\mu{:}\kappa^1$-NHC,S)$(\kappa^1{:}\mu{:}\kappa^1$-P,S)], [trans-$Pt_2Cl_4(\kappa^1{:}\mu{:}\kappa^1$-NHC,S)$(\kappa^1{:}\mu{:}\kappa^1$-P,S)], and [cis-$PtCl_2(\kappa^1{:}\mu{:}\kappa^1$-NHC,S)$(\kappa^1{:}\mu{:}\kappa^1$-P,S)-trans-$PtCl_2(\kappa^1{:}\mu{:}\kappa^1$-NHC,S)$(\kappa^1{:}\mu{:}\kappa^1$-P,S)] (**4a–4c**).* A solution of **3** (81.3 mg, 0.143 mmol) in CD_2Cl_2/CD_3OD (1:1, 2.5 mL) was added to a suspension of complex **2** (115 mg, 0.120 mmol) in CD_2Cl_2/CD_3OD (1:1, 0.7 mL) in a glass vial in the glovebox. The mixture was then stirred at room temperature for 48 h, during which the yellow murky solution became clear and a dark precipitate formed (AgCl). The supernatant was then dried in vacuo to obtain a pale-yellow solid powder as the product (114 mg, 0.0745 mmol, 62% yield). ^1H NMR (400 MHz, CD_2Cl_2): δ 8.06–6.95 (m, 38H), 4.27–3.82 (m, 4H), 3.35–3.10 (br, 8H), 1.26 (s, 6H). ^{31}P NMR (162 MHz, CD_2Cl_2): δ 10.45 (d, $^1J_{P-Pt}$ = 2270 Hz); 9.73 (d, $^1J_{P-Pt}$ = 2300 Hz); 2.53 (d, $^1J_{P-Pt}$ = 2943 Hz); 1.81 (d, $^1J_{P-Pt}$ = 3740 Hz). HRMS (ESI$^+$). Calcd for $[M - Cl]^+$: m/z 1493.1039. Found: m/z 1493.1051.

*[cis-$Pt_2Cl_4(\kappa^1{:}\mu{:}\kappa^1$-NHC,S)$(\kappa^1{:}\mu{:}\kappa^1$-P,S)] (**4a**).* Crystals of complex **4a** were obtained by the slow diffusion of Et_2O into a CH_2Cl_2 solution of **4a–4c**. ^1H NMR (400 MHz, CD_2Cl_2): δ 8.06–8.00 (m, 4H), 7.75 (s, 4H), 7.60–7.48 (m, 10H), 7.35 (s, 4H), 7.30–7.11 (m, 11H), 7.01–6.98 (m, 9H), 6.03–5.84 (d, 13.54 Hz, 2H), 5.78–5.57 (d, 13.51 Hz, 2H), 3.82 (s, 6H), 3.45–3.22 (dt, 6.16, 6.16, 11.32 Hz, 4H), 3.19–2.92 (m, 4H). ^{31}P NMR (162 MHz, CD_2Cl_2): δ 1.84 ($^1J_{P-Pt}$ = 3740 Hz).

DOI: 10.1021/acs.inorgchem.7b02745
Inorg. Chem. 2018, 57, 3568–3578

[cis-Pt$_2$Cl$_2$(κ^1:μ:κ^1-NHC,S)(κ^2:μ:κ^2-P,S)][Cl]$_2$ (**5**). A complex mixture of **4a**–**4c** (or single crystals of **4a**) was fully dried and then dissolved in CD_3OD. ^{1}H NMR (400 MHz, methanol-d_4): δ 8.25 (s, 4H), 7.78–7.60 (m, 12H), 7.57–7.43 (m, 12H), 7.35–7.30 (m, 4H), 7.28 (s, 4H), 7.27–7.24 (m, 2H), 5.51 (d, J = 14.0 Hz, 2H), 4.40 (d, J = 14.0 Hz, 2H), 4.10 (s, 6H), 3.63–3.52 (m, 4H), 3.28–3.11 (m, 4H). ^{31}P NMR (162 MHz, methanol-d_4): δ 36.83(d, $^1J_{P-Pt}$ = 3421 Hz), 36.29. HRMS (ESI$^+$). Calcd for $[M - 2Cl]^{2+}$: m/z 729.0677. Found: m/z 729.0680.

[cis-Pt$_2$(κ^1:μ:κ^2-NHC,S)(κ^2:μ:κ^2-P,S)CD$_3$OD][BF$_4$]$_4$ (**6**). A total of 4 equiv of $AgBF_4$ was added to a solution of **5** in MeOH. The solution was allowed to stir for 30 min. ^{1}H NMR (400 MHz, methanol-d_4): δ 8.54–7.17 (m, 36H), 6.19–5.94 (br, 2H), 4.08–4.02 (s, 2H), 3.68–3.57 (m, 4H), 3.20–2.94 (br, 4H). ^{31}P NMR (162 MHz, methanol-d_4): δ 37.16 (semiopen), 46.95 (fully closed). MALDI-TOF MS (matrix: α-cyano-4-hydroxycinnamic acid). Calcd for $[M + H]^+$: m/z 1767.249. Found: m/z 1767.308.

[cis-Pt$_2$(κ^2:μ:κ^2-NHC,S)(κ^2:μ:κ^2-P,S)][BF$_4$]$_4$ (**7**). Complex **6** was subjected to high vacuum for 2 h to remove the MeOH molecule hypothesized to be bound to the Pt^{II} metal node. The fully dried powder was then dissolved in deuterated nitromethane (CD_3NO_2). ^{1}H NMR (400 MHz, CD_3NO_2): δ 8.51 (s, 4H), 8.16–7.92 (m, 10H), 7.69 (s, 6H), 7.65–7.43 (m, 16H), 6.32–5.84 (m, 4H), 4.02–3.77 (m, 2H), 3.62 (d, J = 19.7 Hz, 6H), 3.34–3.14 (m, 2H), 2.98–2.70 (m, 4H). ^{31}P NMR (162 MHz, CD_3NO_2): δ 50.93 (d, $^1J_{P-Pt}$ = 3450 Hz, diastereomer), δ 49.21 (d, $^1J_{P-Pt}$ = 3450 Hz). MALDI-TOF MS (matrix: 2,5-dihydroxybenzoic acid). Calcd for $[M - BF_4]^+$: m/z 1647.211. Found: m/z 1647.070.

X-ray Crystallography. Single crystals of **2** and **4a** were mounted on a MITIGEN holder in Paratone oil on a Kappa Apex 2 diffractometer. All measurements were made with graphite-monochromated Cu Kα radiation, and all structures were solved with the *ShelXT* structure solution program using direct methods and refined with the *ShelXL* refinement package using least-squares minimization.

■ ASSOCIATED CONTENT

Supporting Information

The Supporting Information is available free of charge on the ACS Publications website at DOI: 10.1021/acs.inorgchem.7b02745.

Experimental details, including VT NMR spectra, reversibility of the structural changes, and NMR and mass spectra (PDF)

Accession Codes

CCDC 1583493–1583494 contain the supplementary crystallographic data for this paper. These data can be obtained free of charge via www.ccdc.cam.ac.uk/data_request/cif, or by emailing data_request@ccdc.cam.ac.uk, or by contacting The Cambridge Crystallographic Data Centre, 12 Union Road, Cambridge CB2 1EZ, UK; fax: +44 1223 336033.

■ AUTHOR INFORMATION

Corresponding Author

*E-mail: chadnano@northwestern.edu.

ORCID

Andrea I. d'Aquino: 0000-0002-4204-8219
Ho Fung Cheng: 0000-0003-2580-0912
Joaquín Barroso-Flores: 0000-0003-0554-7569
C. Michael McGuirk: 0000-0002-7420-1169
Chad A. Mirkin: 0000-0002-6634-7627

Author Contributions

The manuscript was written through contributions of all authors. All authors have given approval to the final version of the manuscript.

Notes

The authors declare no competing financial interest.

■ ACKNOWLEDGMENTS

This material is based on work supported by the National Science Foundation under Grant CHE-1709888 and the U.S. Army under Grant W911NF-15-1-0151. A.I.d. acknowledges a National Science Foundation Graduate Research Fellowship, and J.M.-A. acknowledges a fellowship from Consejo Nacional de Ciencia y Tecnologia (CONACYT). We also thank DGTIC-UNAM for granting access to their supercomputing facilities known as "Miztli".

■ REFERENCES

(1) Fabbrizzi, L.; Poggi, A. Sensors and Switches from Supramolecular Chemistry. *Chem. Soc. Rev.* **1995**, *24*, 197–202.
(2) Ashton, P. R.; Balzani, V.; Becher, J.; Credi, A.; Fyfe, M. C. T.; Mattersteig, G.; Menzer, S.; Nielsen, M. B.; Raymo, F. M.; Stoddart, J. F.; Venturi, M.; Williams, D. J. A three-pole supramolecular switch. *J. Am. Chem. Soc.* **1999**, *121*, 3951–3957.
(3) Cook, T. R.; Stang, P. J. Coordination-Driven Supramolecular Macromolecules via the Directional Bonding Approach. *Adv. Polym. Sci.* **2013**, *261*, 229–248.
(4) Yoshizawa, M.; Klosterman, J. K.; Fujita, M. Functional Molecular Flasks: New Properties and Reactions within Discrete, Self-Assembled Hosts. *Angew. Chem., Int. Ed.* **2009**, *48*, 3418–3438.
(5) Caulder, D. L.; Raymond, K. N. The rational design of high symmetry coordination clusters. *J. Chem. Soc., Dalton Trans.* **1999**, 1185–1200.
(6) Caulder, D. L.; Raymond, K. N. Supermolecules by design. *Acc. Chem. Res.* **1999**, *32*, 975–982.
(7) Smulders, M. M. J.; Riddell, I. A.; Browne, C.; Nitschke, J. R. Building on architectural principles for three-dimensional metallosupramolecular construction. *Chem. Soc. Rev.* **2013**, *42*, 1728–1754.
(8) Ronson, T. K.; Zarra, S.; Black, S. P.; Nitschke, J. R. Metal-organic container molecules through subcomponent self-assembly. *Chem. Commun.* **2013**, *49*, 2476–2490.
(9) Oliveri, C. G.; Nguyen, S. T.; Mirkin, C. A. A highly modular and convergent approach for the synthesis of stimulant-responsive heteroligated cofacial porphyrin tweezer complexes. *Inorg. Chem.* **2008**, *47*, 2755–2763.
(10) Lifschitz, A. M.; Rosen, M. S.; McGuirk, C. M.; Mirkin, C. A. Allosteric Supramolecular Coordination Constructs. *J. Am. Chem. Soc.* **2015**, *137*, 7252–7261.
(11) Kennedy, R. D.; Machan, C. W.; McGuirk, C. M.; Rosen, M. S.; Stern, C. L.; Sarjeant, A. A.; Mirkin, C. A. General Strategy for the Synthesis of Rigid Weak-Link Approach Platinum(II) Complexes: Tweezers, Triple-Layer Complexes, and Macrocycles. *Inorg. Chem.* **2013**, *52*, 5876–5888.
(12) Yamanaka, M.; Yamada, Y.; Sei, Y.; Yamaguchi, K.; Kobayashi, K. Selective formation of a self-assembling homo or hetero cavitand cage via metal coordination based on thermodynamic or kinetic control. *J. Am. Chem. Soc.* **2006**, *128*, 1531–1539.
(13) Schmittel, M.; Mahata, K. Diversity and complexity through reversible multiple orthogonal interactions in multicomponent assemblies. *Angew. Chem., Int. Ed.* **2008**, *47*, 5284–5286.
(14) Dalgarno, S. J.; Power, N. P.; Atwood, J. L. Metallo-supramolecular capsules. *Coord. Chem. Rev.* **2008**, *252*, 825–841.
(15) Wiester, M. J.; Ulmann, P. A.; Mirkin, C. A. Enzyme Mimics Based Upon Supramolecular Coordination Chemistry. *Angew. Chem., Int. Ed.* **2011**, *50*, 114–137.
(16) Mendez-Arroyo, J.; d'Aquino, A. I.; Chinen, A. B.; Manraj, Y. D.; Mirkin, C. A. Reversible and Selective Encapsulation of Dextromethorphan and beta-Estradiol Using an Asymmetric Molecular Capsule Assembled via the Weak-Link Approach. *J. Am. Chem. Soc.* **2017**, *139*, 1368–1371.

DOI: 10.1021/acs.inorgchem.7b02745
Inorg. Chem. 2018, 57, 3568–3578

(17) Mendez-Arroyo, J.; Barroso-Flores, J.; Lifschitz, A. M.; Sarjeant, A. A.; Stern, C. L.; Mirkin, C. A. A Multi-State, Allosterically-Regulated Molecular Receptor With Switchable Selectivity. *J. Am. Chem. Soc.* **2014**, *136*, 10340−10348.
(18) Gianneschi, N. C.; Masar, M. S., 3rd; Mirkin, C. A. Development of a coordination chemistry-based approach for functional supramolecular structures. *Acc. Chem. Res.* **2005**, *38*, 825−837.
(19) McGuirk, C. M.; Stern, C. L.; Mirkin, C. A. Small Molecule Regulation of Self-Association and Catalytic Activity in a Supramolecular Coordination Complex. *J. Am. Chem. Soc.* **2014**, *136*, 4689−4696.
(20) McGuirk, C. M.; Mendez-Arroyo, J.; Lifschitz, A. M.; Mirkin, C. A. Allosteric Regulation of Supramolecular Oligomerization and Catalytic Activity via Coordination-Based Control of Competitive Hydrogen-Bonding Events. *J. Am. Chem. Soc.* **2014**, *136*, 16594−16601.
(21) Yoon, H. J.; Kuwabara, J.; Kim, J. H.; Mirkin, C. A. Allosteric Supramolecular Triple-Layer Catalysts. *Science* **2010**, *330*, 66−69.
(22) Ulmann, P. A.; Braunschweig, A. B.; Lee, O. S.; Wiester, M. J.; Schatz, G. C.; Mirkin, C. A. Inversion of product selectivity in an enzyme-inspired metallosupramolecular tweezer catalyzed epoxidation reaction. *Chem. Commun.* **2009**, 5121−5123.
(23) McGuirk, C. M.; Mendez-Arroyo, J.; d'Aquino, A. I.; Stern, C. L.; Liu, Y.; Mirkin, C. A. A concerted two-prong approach to the in situ allosteric regulation of bifunctional catalysis. *Chem. Sci.* **2016**, *7*, 6674−6683.
(24) Lifschitz, A. M.; Young, R. M.; Mendez-Arroyo, J.; Stern, C. L.; McGuirk, C. M.; Wasielewski, M. R.; Mirkin, C. A. An allosteric photoredox catalyst inspired by photosynthetic machinery. *Nat. Commun.* **2015**, *6*, 6541.
(25) Lifschitz, A. M.; Young, R. M.; Mendez-Arroyo, J.; Roznyatovskiy, V. V.; McGuirk, C. M.; Wasielewski, M. R.; Mirkin, C. A. Chemically regulating Rh(I)-Bodipy photoredox switches. *Chem. Commun.* **2014**, *50*, 6850−6852.
(26) Masar, M. S.; Mirkin, C. A.; Stern, C. L.; Zakharov, L. N.; Rheingold, A. L. Binuclear copper(I) macrocycles synthesized via the weak-link approach. *Inorg. Chem.* **2004**, *43*, 4693−4701.
(27) Machan, C. W.; Spokoyny, A. M.; Jones, M. R.; Sarjeant, A. A.; Stern, C. L.; Mirkin, C. A. Plasticity of the Nickel(II) Coordination Environment in Complexes with Hemilabile Phosphino Thioether Ligands. *J. Am. Chem. Soc.* **2011**, *133*, 3023−3033.
(28) Kuwabara, J.; Ovchinnikov, M. V.; Stern, C. L.; Mirkin, C. A. Reactivity of dinuclear rhodium(I) macrocycles formed via the weak-link approach. *Organometallics* **2008**, *27*, 789−792.
(29) Khoshbin, M. S.; Ovchinnikov, M. V.; Mirkin, C. A.; Zakharov, L. N.; Rheingold, A. L. Binuclear ruthenium macrocycles formed via the weak-link approach. *Inorg. Chem.* **2005**, *44*, 496−501.
(30) Rosen, M. S.; Stern, C. L.; Mirkin, C. A. Heteroligated Pt-II Weak-Link Approach complexes using hemilabile N-heterocyclic carbene-thioether and phosphino-thioether ligands. *Chem. Sci.* **2013**, *4*, 4193−4198.
(31) Yoo, H.; Rosen, M. S.; Brown, A. M.; Wiester, M. J.; Stern, C. L.; Mirkin, C. A. Elucidating the Mechanism of the Halide-Induced Ligand Rearrangement Reaction. *Inorg. Chem.* **2012**, *51*, 11986−11995.
(32) Oliveri, C. G.; Ulmann, P. A.; Wiester, M. J.; Mirkin, C. A. Heteroligated Supramolecular Coordination Complexes Formed via the Halide-Induced Ligand Rearrangement Reaction. *Acc. Chem. Res.* **2008**, *41*, 1618−1629.
(33) Krevor, J. V. Z.; Simonis, U.; Richter, J. A. Structural-Analysis of Platinum Phosphine Complexes by 2-Dimensional P-31 Nmr-Spectroscopy. *Inorg. Chem.* **1992**, *31*, 2409−2414.
(34) Pregosin, P. S. Pt-195 Nuclear Magnetic-Resonance. *Coord. Chem. Rev.* **1982**, *44*, 247−291.
(35) Still, B. M.; Kumar, P. G.; Aldrich-Wright, J. R.; Price, W. S. 195Pt NMR–theory and application. *Chem. Soc. Rev.* **2007**, *36*, 665−686.
(36) Kennedy, R. D.; Stern, C. L.; Mirkin, C. A. Zwitterionic Weak-Link Approach Complexes Based on Anionic Icosahedral Monocarbaboranes. *Inorg. Chem.* **2013**, *52*, 14064−14071.
(37) Wiester, M. J.; Braunschweig, A. B.; Yoo, H.; Mirkin, C. A. Solvent and Temperature Induced Switching Between Structural Isomers of Rh-I Phosphinoalkyl Thioether (PS) Complexes. *Inorg. Chem.* **2010**, *49*, 7188−7196.
(38) Macchioni, A. Ion pairing in transition-metal organometallic chemistry. *Chem. Rev.* **2005**, *105*, 2039−2073.
(39) Garrou, P. E. Delta-R Ring Contributions to P-31 Nmr Parameters of Transition-Metal-Phosphorus Chelate Complexes. *Chem. Rev.* **1981**, *81*, 229−266.
(40) Abel, E. W.; Bhargava, S. K.; Orrell, K. G. The Stereodynamics of Metal-Complexes of Sulfur-Containing, Selenium-Containing, and Tellurium-Containing Ligands. *Prog. Inorg. Chem.* **1984**, *32*, 1−118.
(41) Abel, E. W.; Bhargava, S. K.; Kite, K.; Orrell, K. G.; Sik, V.; Williams, B. L. Structural Dependencies of Pyramidal Inversion at Sulfur and Selenium in Thio-Ether and Seleno-Ether Complexes of Palladium(Ii) and Platinum(Ii) - a Nuclear Magnetic-Resonance Study. *Polyhedron* **1982**, *1*, 289−298.
(42) Ulmann, P. A.; Brown, A. M.; Ovchinnikov, M. V.; Mirkin, C. A.; DiPasquale, A. G.; Rheingold, A. L. Spontaneous formation of heteroligated Pt-II complexes with chelating hemilabile ligands. *Chem. - Eur. J.* **2007**, *13*, 4529−4534.
(43) Noda, K.; Sasaki, T.; Iwatsuki, S.; Kashiwabara, K.; Suzuki, T.; Takagi, H. D. Syntheses and first structural analyses of Cu(I)-PS complexes with bidentate 1,1-diphenyl-1-phospha-4-thiapentane (mtdpp) and quadridentate 5,9-diphenyl-5,9-diphospha-2,12-dithiatridecane (2,3,2-SPPS): successful synthetic route for monomeric [Cu(mtdpp)2]BF4 and dimeric [Cu-2(2,3,2-SPPS)(2)](BF4)(2). *Inorg. Chim. Acta* **2004**, *357*, 526−532.

DOI: 10.1021/acs.inorgchem.7b02745
Inorg. Chem. 2018, 57, 3568−3578

Supporting Information

An Allosterically-Regulated, Four-State Macrocycle

*Andrea I. d'Aquino,[†] Ho Fung Cheng,[†] Joaquín Barroso-Flores,[§] Zachary S. Kean,[†] Jose Mendez-Arroyo,[†] C. Michael McGuirk,[†] Chad A. Mirkin**

* To whom correspondences should be addressed

†Department of Chemistry and International Institute for Nanotechnology, Northwestern University, 2145 Sheridan Road, Evanston, Illinois 60208, United States

§ Centro Conjunto de Investigación en Química Sustentable, UAEM-UNAM, Carretera Toluca-Atlacomulco Km 14.5, Personal de la UNAM, Unidad San Cayetano, Toluca, Estado de México C. P. 50200, México

Table of Contents

^{1}H DOSY of complex 5

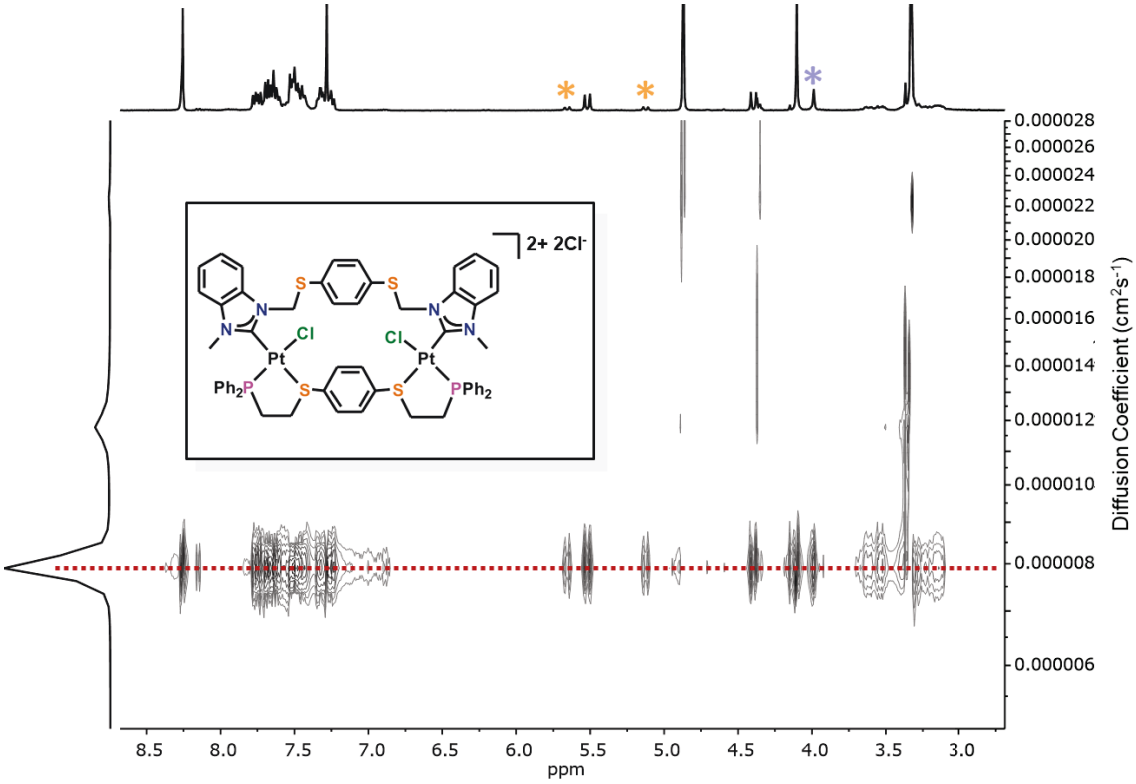

Figure S1. ^{1}H DOSY NMR spectra of a sample containing complex *5* in methanl-d_4. The region corresponding to the semi-open species is indicated by the dotted red line. Asterisks denotes a diastereomer of *5*. The average diffusion coefficient of complex *5* in methanol, was determined to be $8x10^{-6}$ cm^2s^{-1}.

Variable Temperature NMR Spectra of 7

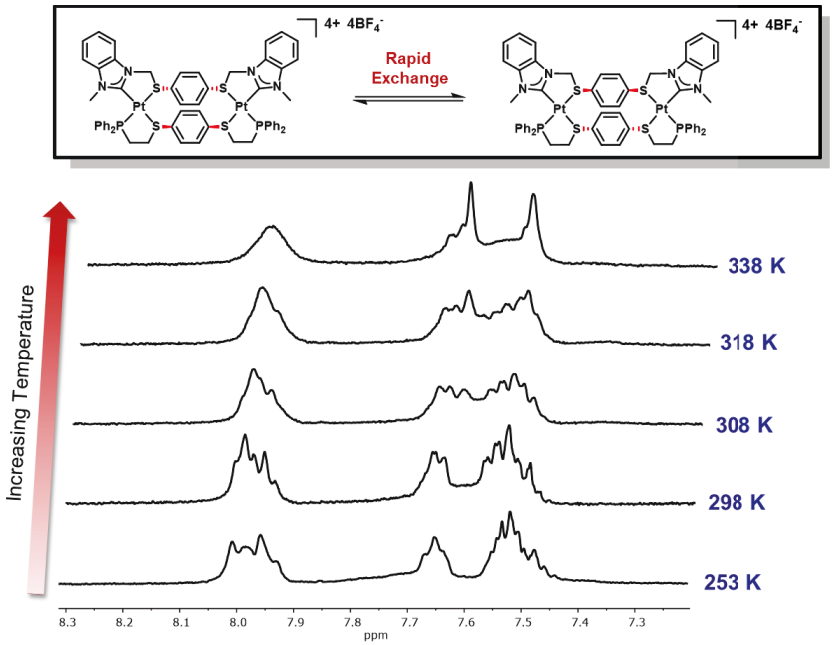

Figure S2. ^{1}H NMR spectra of complex *7* in CD_3NO_2 from 253 K to 338 K. Coalescence is observed at high temperature, consistent with the presence of rapidly interconverting diastereomers at elevated temperature.

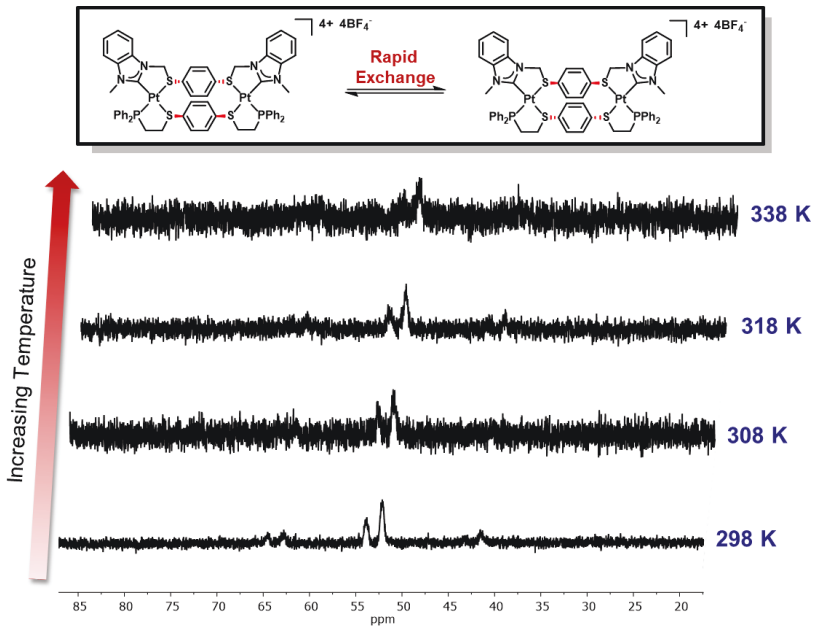

Figure S3. ^{31}P NMR spectra of complex *7* in CD_3NO_2 from 253 K to 338 K. Coalescence is observed at high temperature, consistent with the presence of rapidly interconverting diastereomers at elevated temperature.

Density Functional Theory Calculations

All structures were optimized at the B97D/lanl2dz level of theory. Functional B97D includes dispersion effects albeit empirically. The Lanl2dz basis set was used with a pseudopotential for Pt^{II} and Cl because we can expand their core electrons and include some relativistic affects when studying the platinum bonding. Population analysis was performed within the Natural Bond Orbitals (NBO) formalism. NBO allows for a localized, pairwise, description of the electron density and is more reliable than the Mulliken's default. Interaction energies were calculated with the NBODel (deletion) procedure. This takes the Fock matrix and finds the elements that connect orbitals from one atom to those of another and sets their values to zero (deletion); the resulting matrix is re-diagonalized and the associated energy value increases with respect to the original non-deleted one. The change in energy is ascribed to the interaction energy.

Energy Minimized Models of 5, 6 and 7

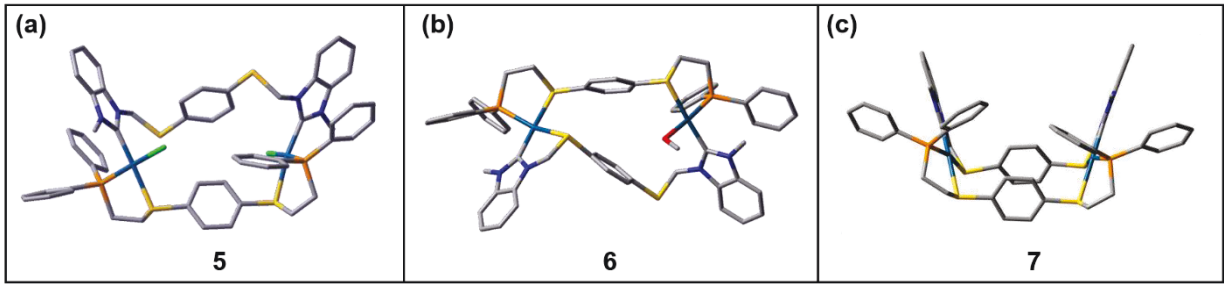

Figure S4. Energy minimized DFT models of (a) semi-open complex *5*, (b) semi-open/fully closed complex *6*, and (c) fully closed complex *7*.

Table S1. Free Energies (kcal/mol) of *5*, *6* and *7* Obtained from DFT Calculations.

Compound	*Free Energy (kcal/mol)*
5	-2780.8563
6	-2865.6565
7	-2750.0284

Bond Energies Calculated for 5, 6 and 7

Table S2. Selected Bond Energies (kcal/mol) of *5*, *6* and *7* Obtained from DFT Calculations.

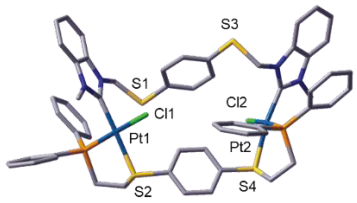 **5**		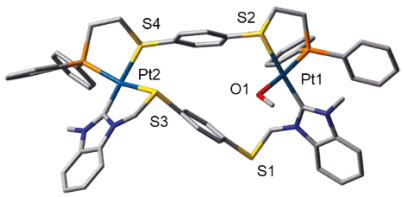 **6**		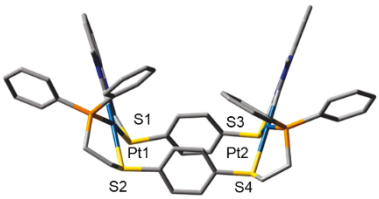 **7**	
Bond	*Δ Energy (kcal/mol)*	*Bond*	*Δ Energy (kcal/mol)*	*Bond*	*Δ Energy (kcal/mol)*
Pt1–S2	61.239	Pt1–S2	42.255	Pt1–S1	59.529
Pt1–Cl1	88.486	Pt1–O1	30.704	Pt1–S2	63.514
Pt2–S4	62.264	Pt2–S4	63.771	Pt2–S3	64.226
Pt2–Cl2	92.227	Pt2–S3	57.102	Pt2–S4	58.440

Fukui Indices Calculated for Complex 5

Table S3. Selected Fukui Indices for *5* Obtained from DFT Calculations.[a]

Atom	Fukui Indice
Cl1	**0.54**
Cl2	**0.54**
Pt1	**0.045**
Pt2	**0.051**
S1	**0.13**
S3	**0.14**

[a]Fukui indices indicate the electrophilic and nucleophilic sites. Electrophilic sites are highlighted in blue in Table S3, while nucleophilic sites are highlighted in red.

Diastereomers of 5 and 7

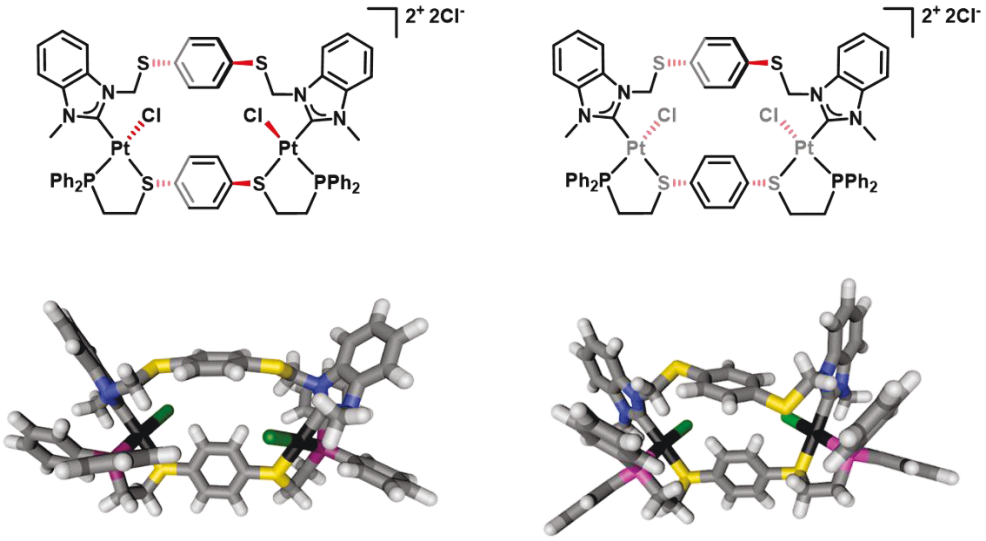

Figure S5. ChemDraw structures (top) and corresponding DFT models (bottom) showing the two possible diastereomers of *5*.

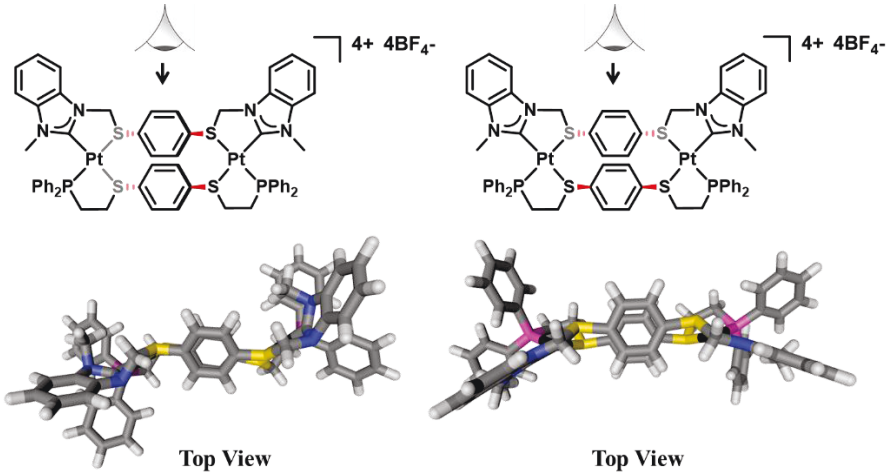

Figure S6. ChemDraw structures (top) and corresponding DFT models (bottom) showing top-down views of the two possible diastereomers of *7*.

Crystallographic Data

Suitable crystals were selected and the crystals were each mounted on MITIGEN holders in Paratone oil on a Kappa Apex 2 diffractometer. Using Olex2,[1] the structures were solved with the ShelXT[2] structure solution program using Direct Methods and refined with the ShelXL[3] refinement package using Least Squares minimization.

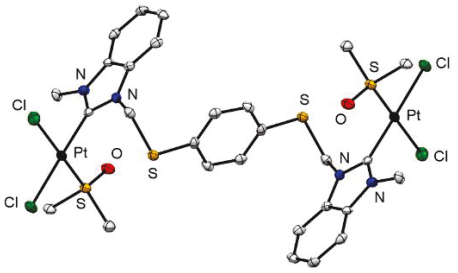

2-DMSO

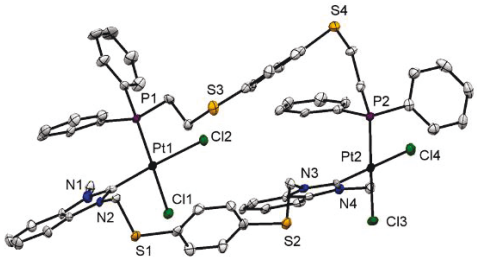

4a

Table S4. Crystallographic Data for Complex *2-DMSO* and *4a.*

	2-DMSO	*4a*
Empirical formula	$C_{40}H_{70}Cl_4N_4O_8Pt_2S_{10}$	$C_{62}H_{62}Cl_{12}N_4P_2Pt_2S_4$
Formula weight	1587.58	1868.91
Temperature / K	100.06	100.0
Crystal system	triclinic	triclinic
Space group	P-1	P-1
a / Å	9.2837(3)	11.3838(5)
b / Å	11.1950(4)	17.4837(7)
c / Å	14.3816(5)	18.1658(8)
α/°	91.703(2)	84.972(3)
β/°	90.044(2)	74.501(3)
γ/°	104.747(2)	79.960(3)
Volume / $Å^3$	1444.77(9)	3427.5(3)
Z	1	2
ρ_{calc} / mg mm^{-3}	1.825	1.811
μ / mm^{-1}	14.412	13.749
F(000)	786	1832

Crystal size / mm^3	0.253 × 0.164 × 0.015	0.212 × 0.025 × 0.015
2Θ range for data collection	6.148 to 130.288°	7.05 to 133.55°
Index ranges	$-10 \leq h \leq 10, -13 \leq k \leq 12, -16 \leq l \leq 16$	$-12 \leq h \leq 13, -20 \leq k \leq 20, 0 \leq l \leq 21$
Reflections collected	11518	11971
Independent reflections	4844[R(int) = 0.0334]	11971[R(int) = 0.0731]
Data/restraints/parameters	4844/0/316	11971/0/777
Goodness-of-fit on F^2	1.044	1.077
Final R indexes [I>2σ (I)]	$R_1 = 0.0317$, $wR_2 = 0.0939$	$R_1 = 0.0464$, $wR_2 = 0.1028$
Final R indexes [all data]	$R_1 = 0.0331$, $wR_2 = 0.0952$	$R_1 = 0.0667$, $wR_2 = 0.1093$
Largest diff. peak/hole / e $Å^{-3}$	2.338/-1.249	2.399/-1.460

Reversible Opening and Closing of the WLA Macrocycle

General procedure for re-opening 6 to form semi-open macrocycle 5. Four equivalents of bis(triphenylphosphoranylidene)ammonium chloride (PPNCl) was added to a sample of complex **6** in methanol-d_4.

General procedure for re-opening 5 to form fully open macrocycle 4a. Fully dried complex **5** was dissolved in CD_2Cl_2 to form complex **4a**.

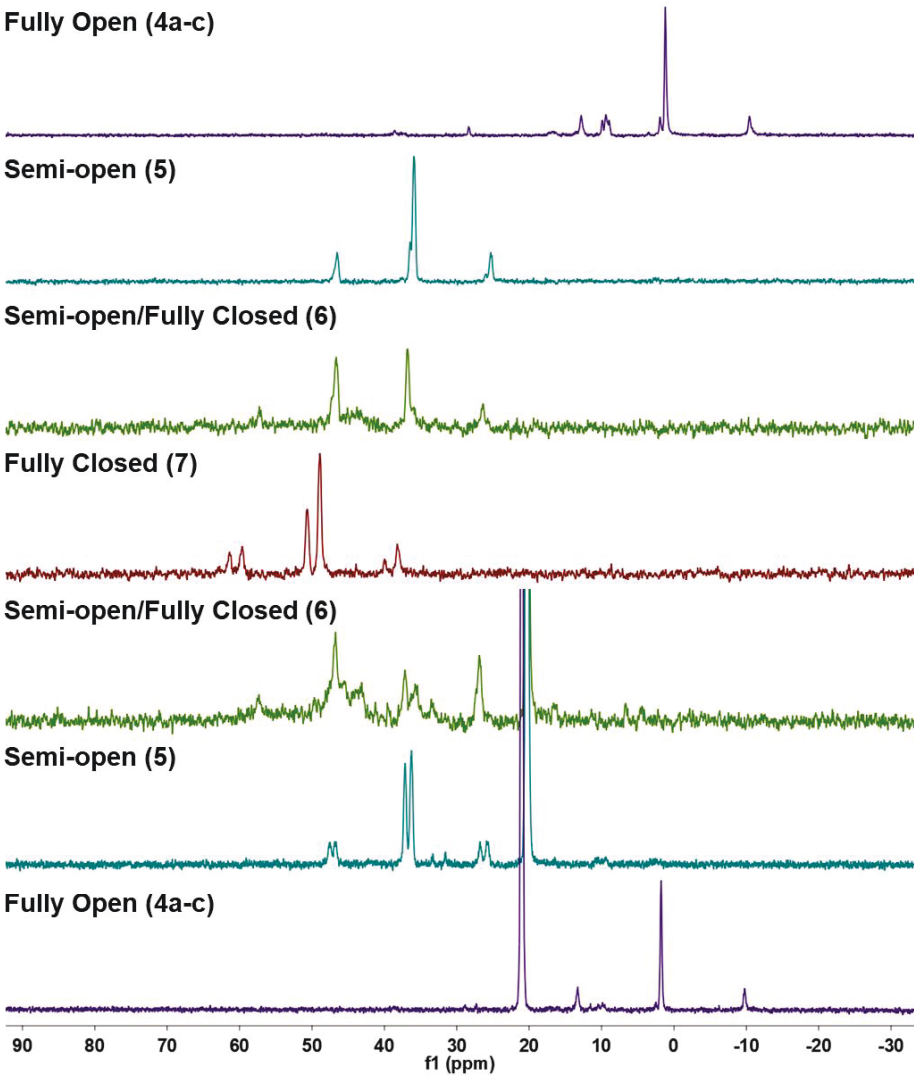

Figure S7. ^{31}P NMR spectra of complexes **4a-c**, **5**, and **6** upon reopening and closing.

NMR Spectra

Benzimidazolium chloride salt (1)

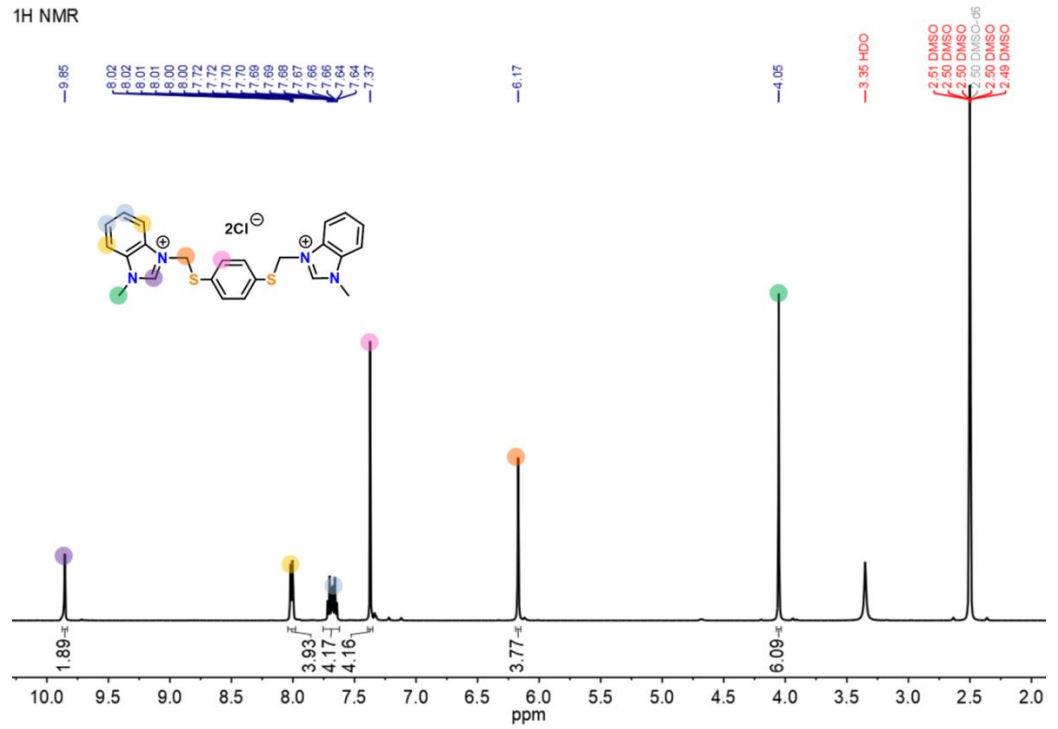

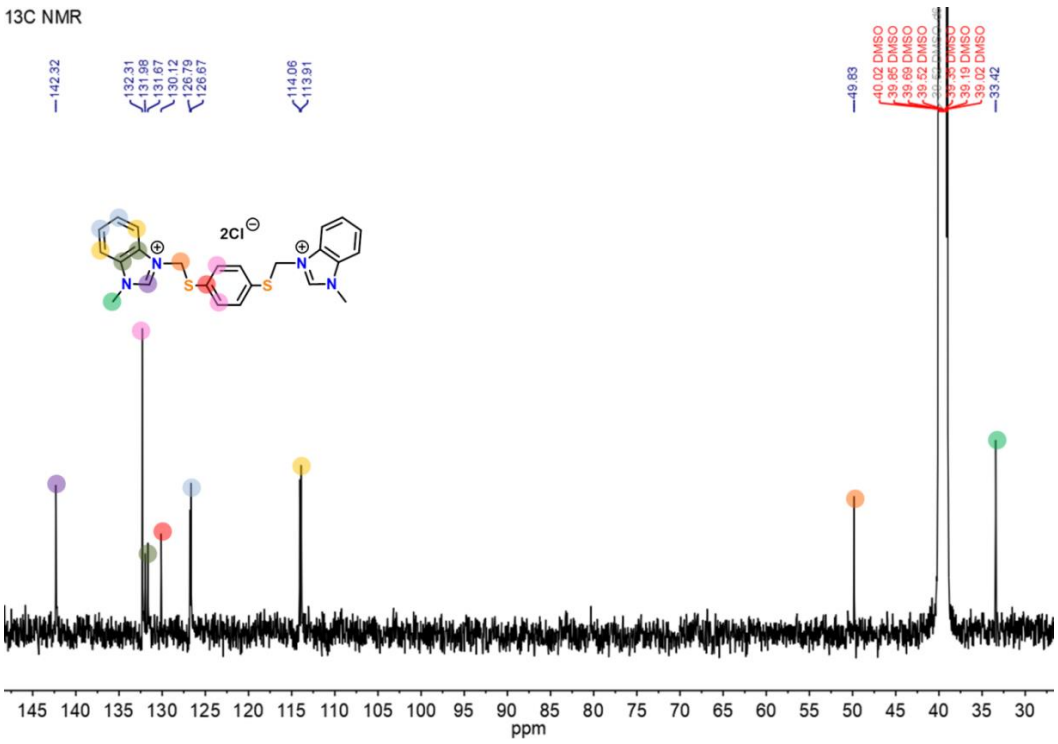

Monoligated Complex [$Pt_2Cl_4(\kappa^1:\mu:\kappa^1$–NHC,S)$(C_2H_6OS)_2$] (2-DMSO)

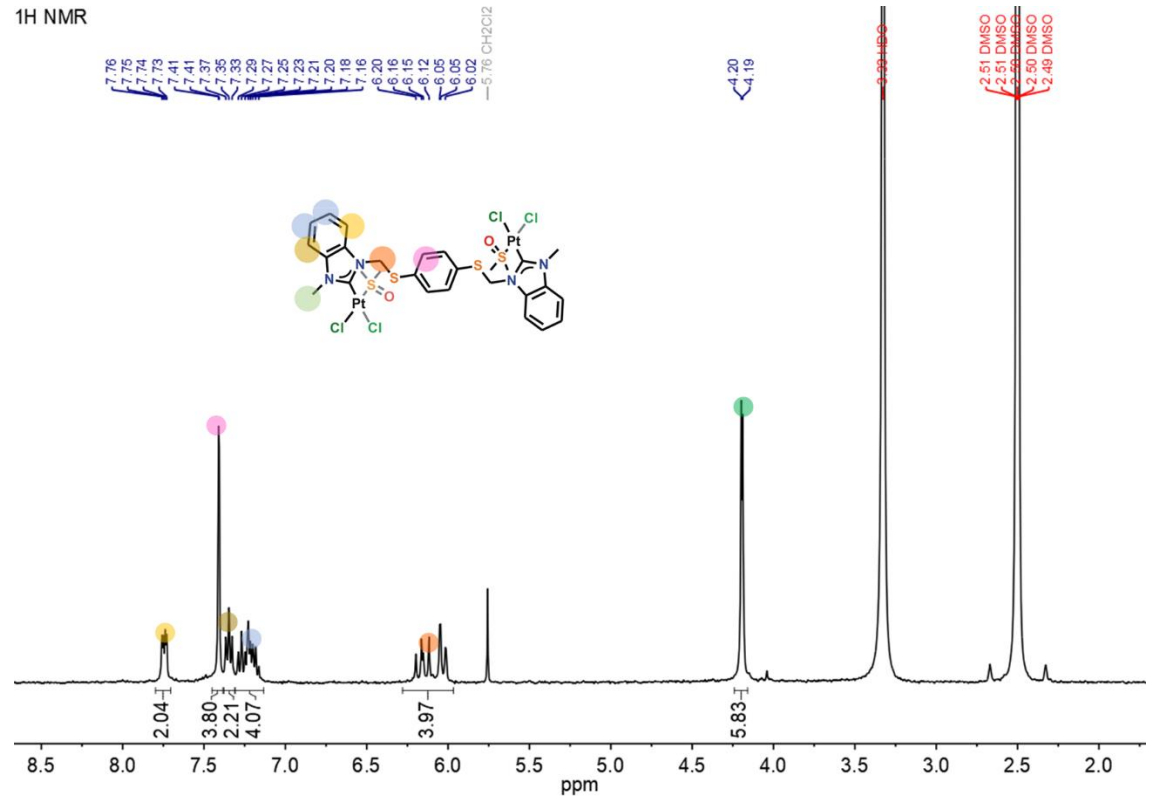

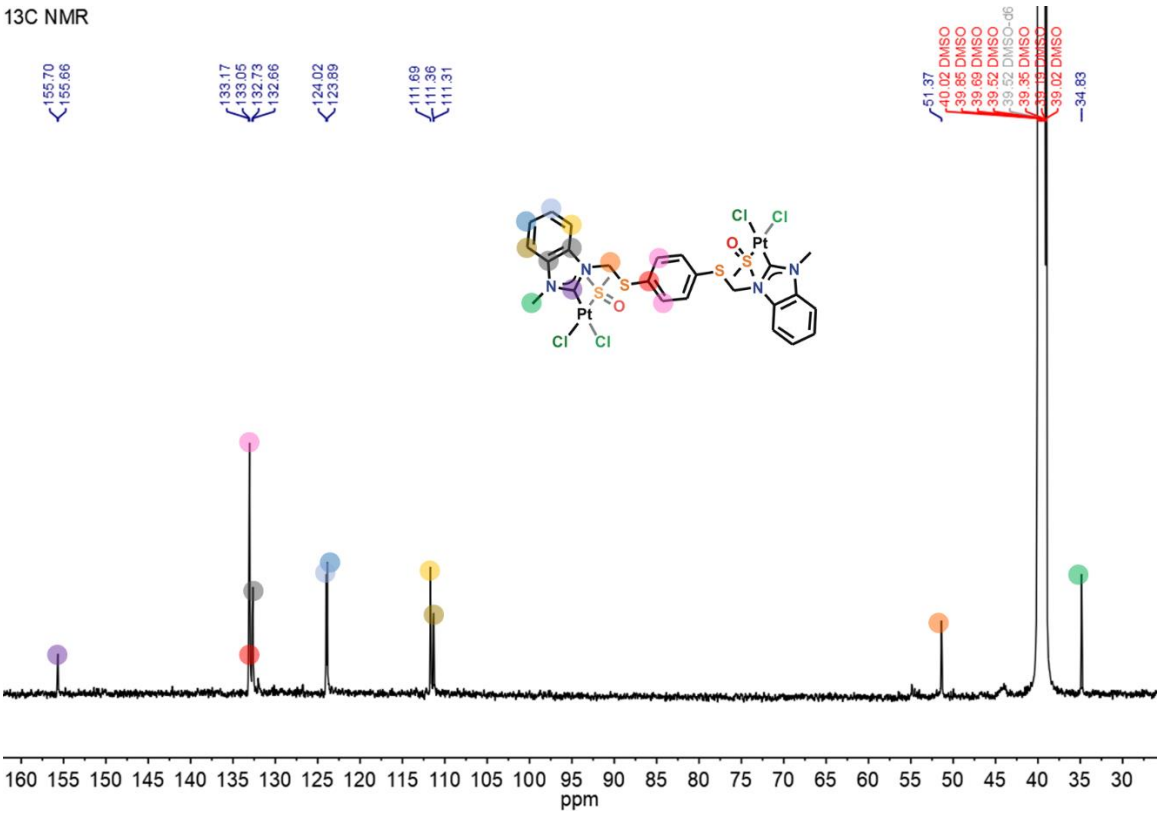

1,4-bis(diphenylphosphino)ethyl thiob enzene (3)

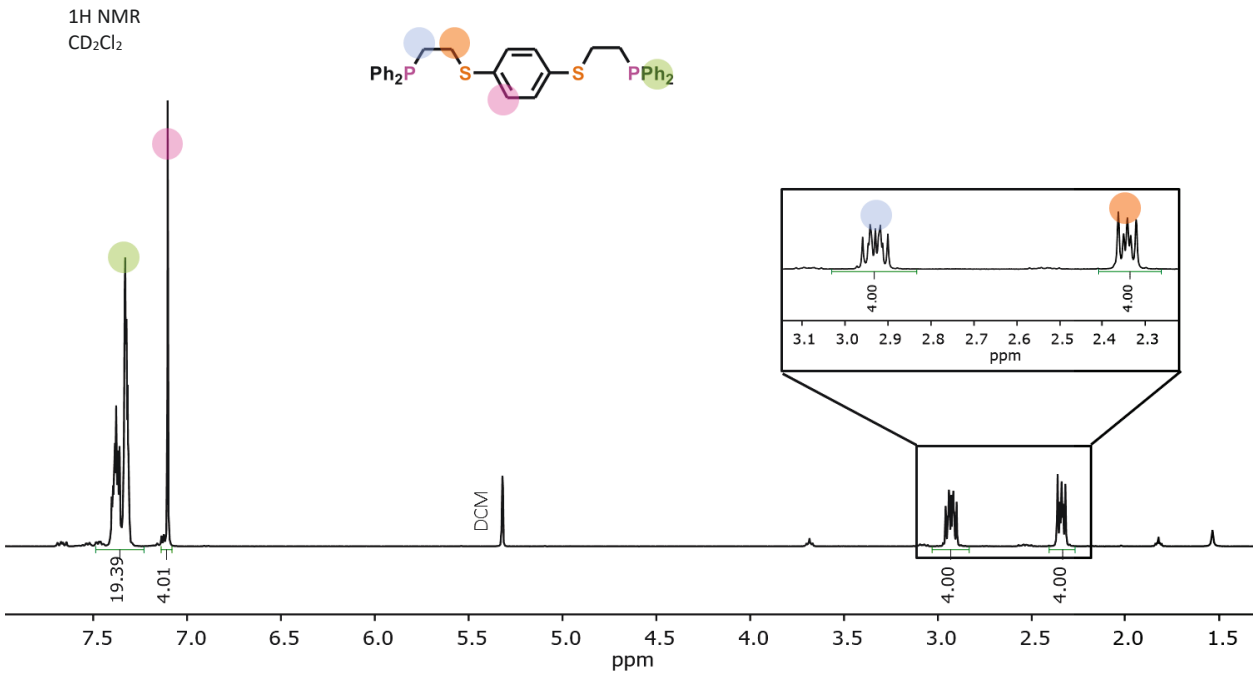

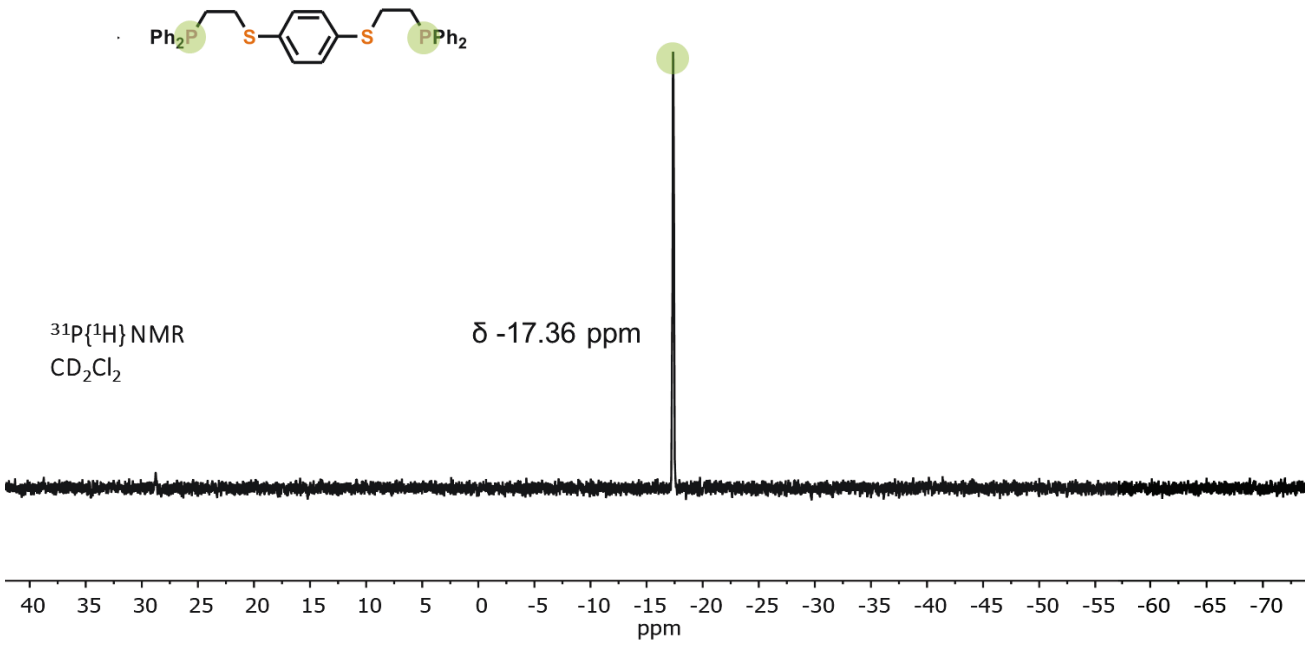

Fully Open Macrocycle Isomers (4a-c)

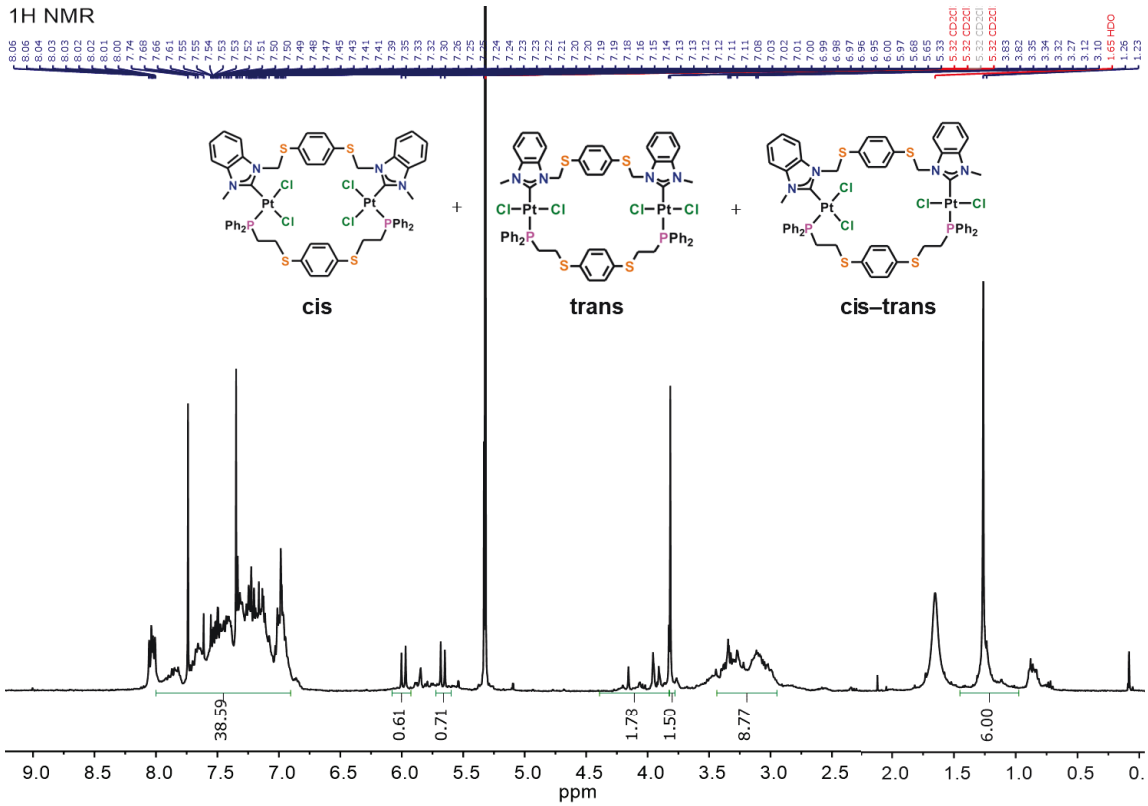

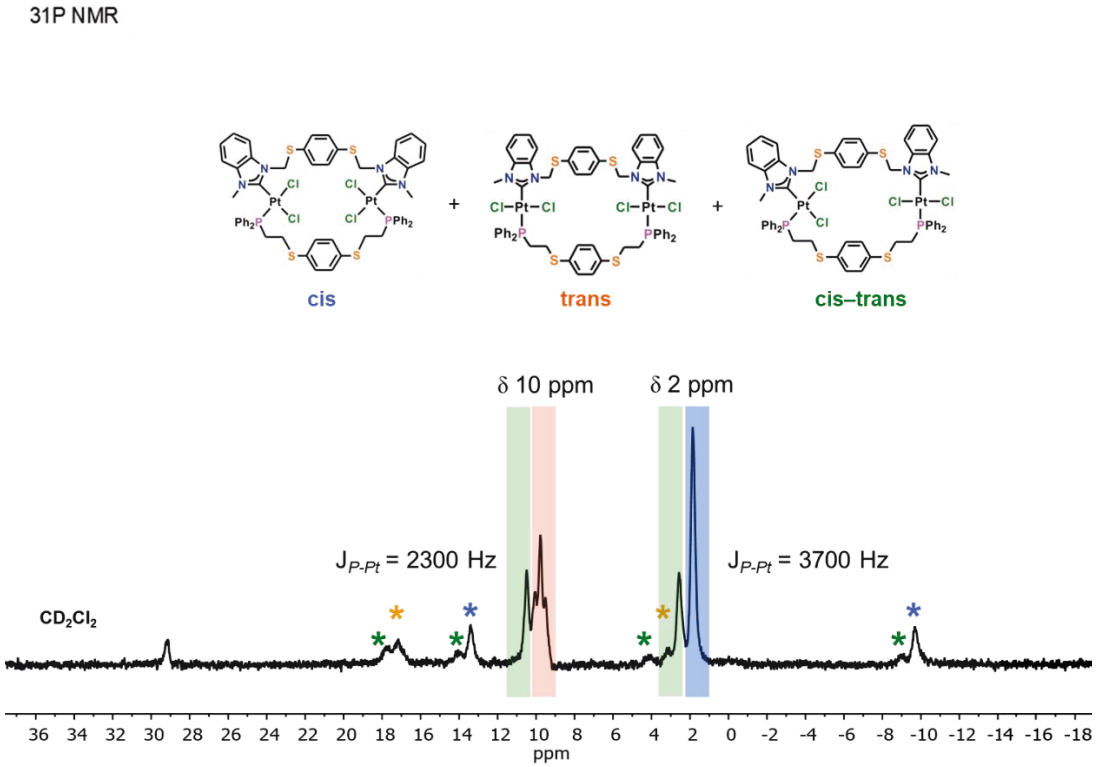

Fully Open Macrocycle Crystals [cis–Pt_2Cl_4(κ^1:μ:κ^1–NHC,S)(κ^1:μ:κ^1–P,S)] (4a)

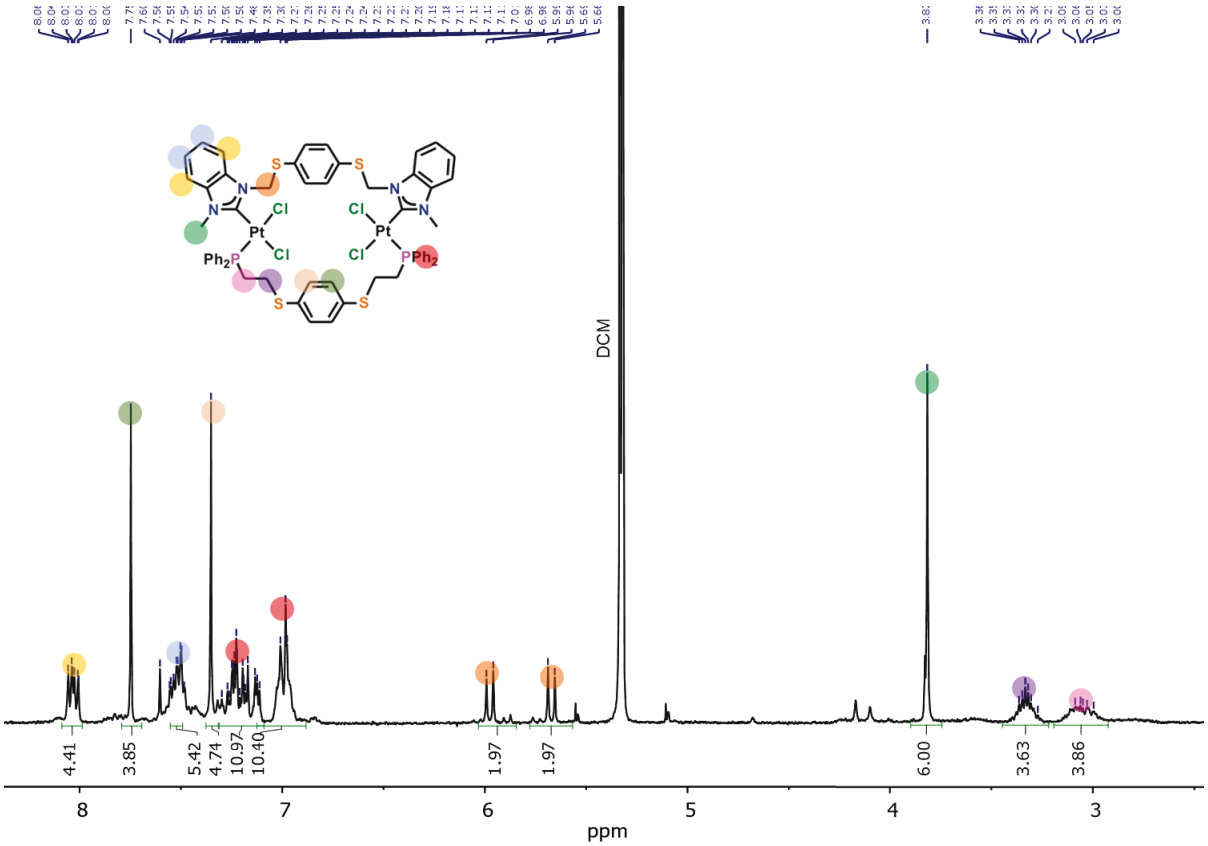

31P NMR

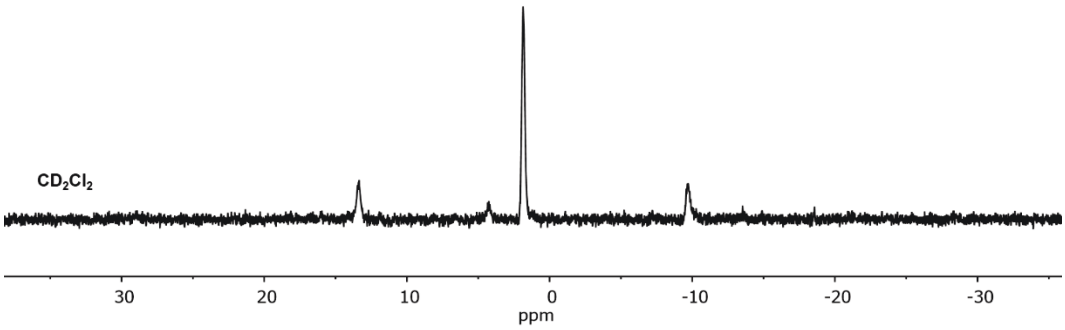

Semi-Open Complex [*cis*–$Pt_2Cl_2(\kappa^1{:}\mu{:}\kappa^1$–NHC,S)($\kappa^2{:}\mu{:}\kappa^2$–P,S)][Cl]$_2$ (5)

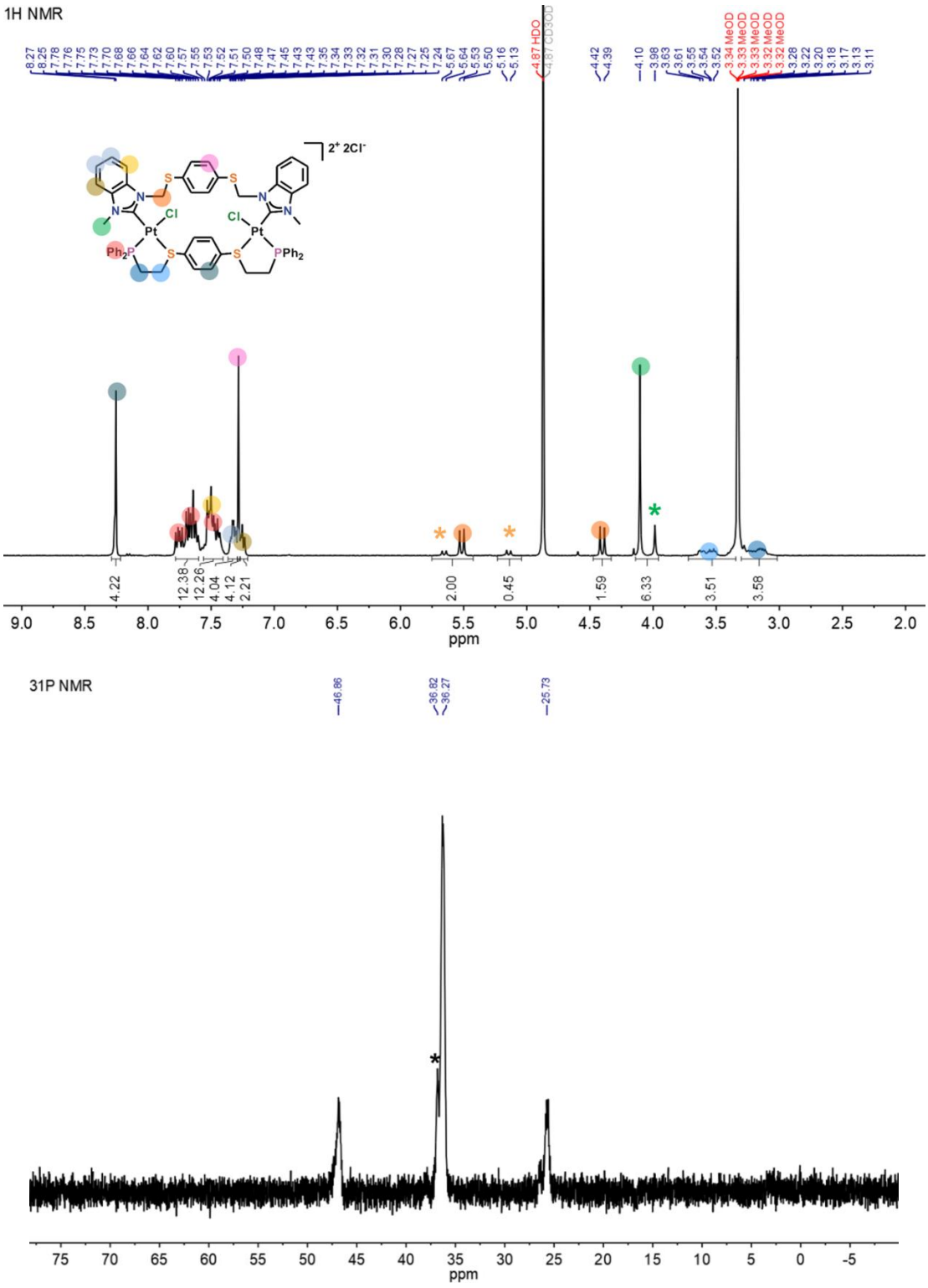

*Diastereomer of **5**.

Fully Closed/Semi-Open Complex [*cis*–$Pt_2(\kappa^1{:}\mu{:}\kappa^2$–NHC,S)($\kappa^2{:}\mu{:}\kappa^2$–P,S)$CD_3OD][BF_4]_4$ (6)

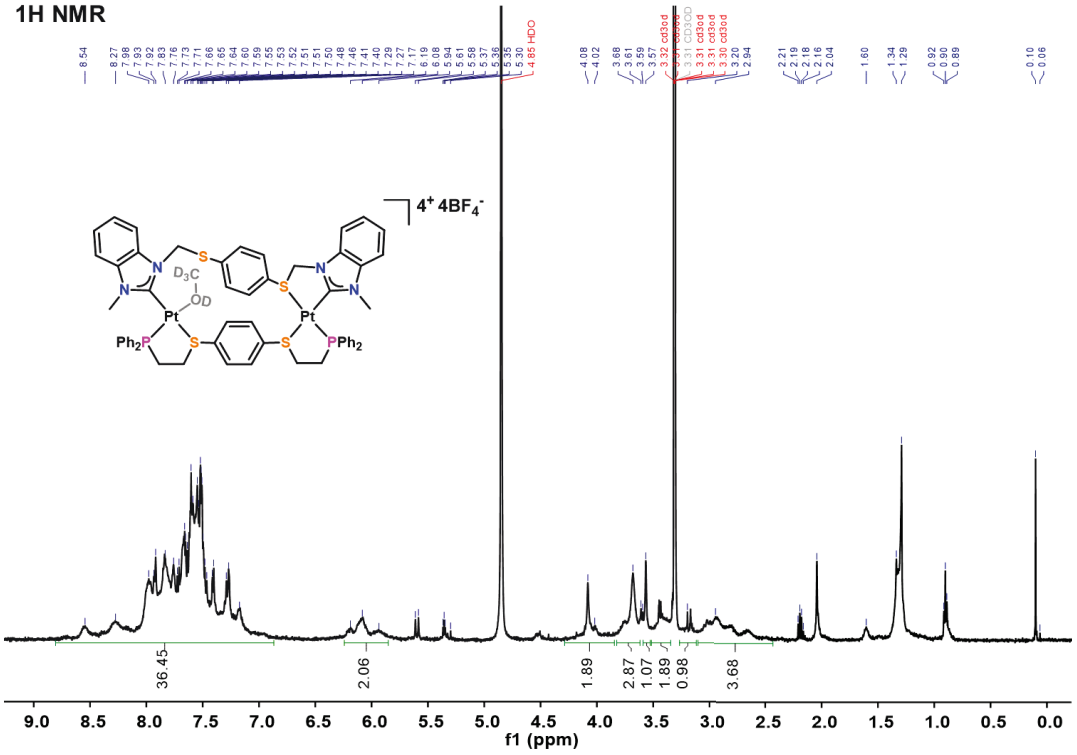

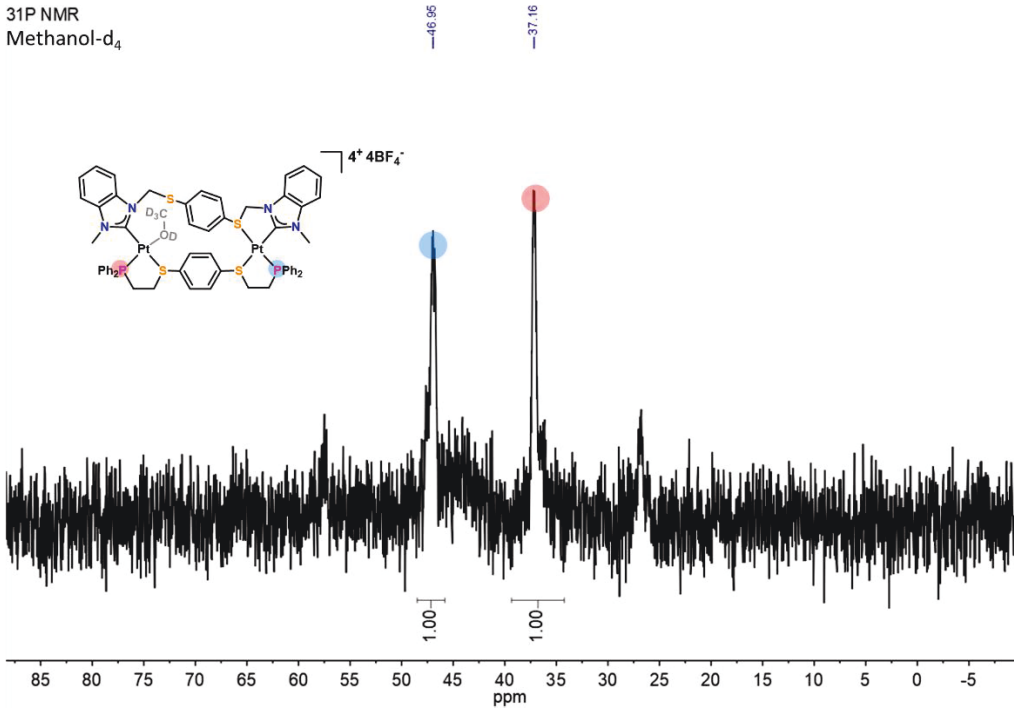

Fully Closed Macrocycle [*cis*–Pt$_2$(κ^2:μ:κ^2–NHC,S)(κ^2:μ:κ^2–P,S)][BF$_4$]$_4$ (7)

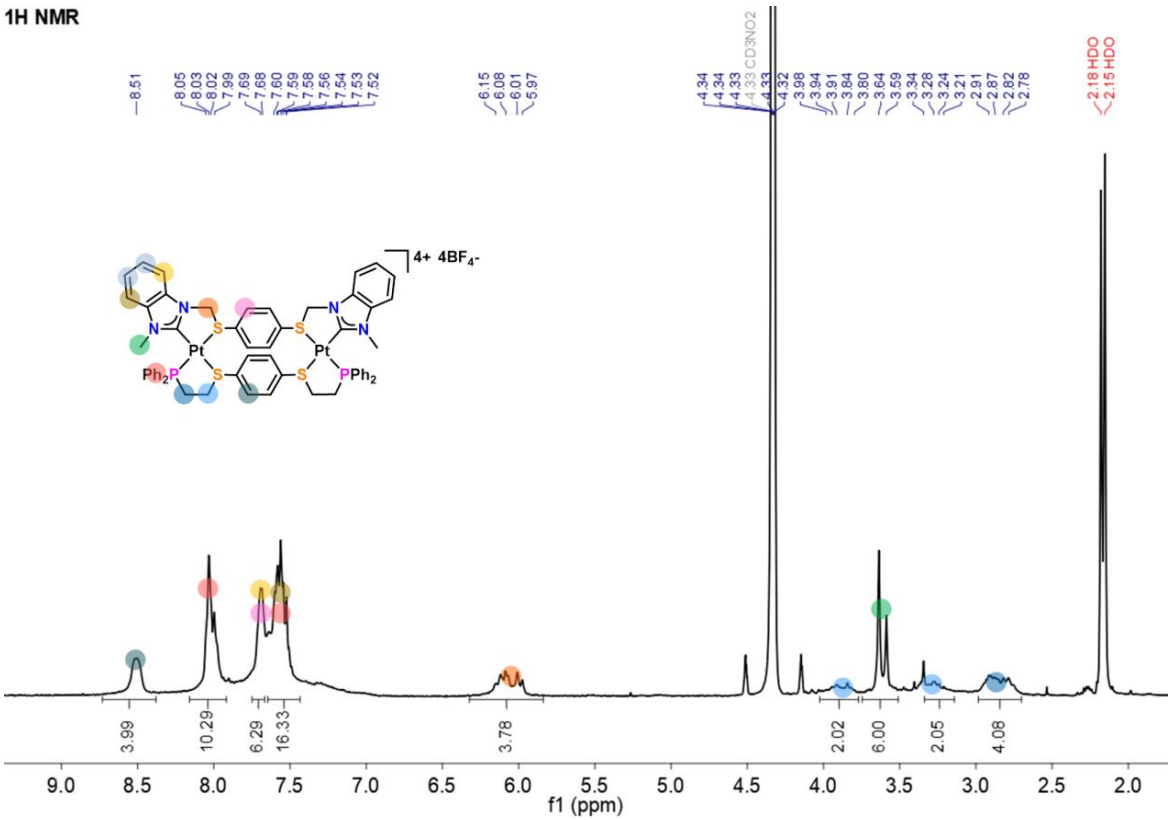

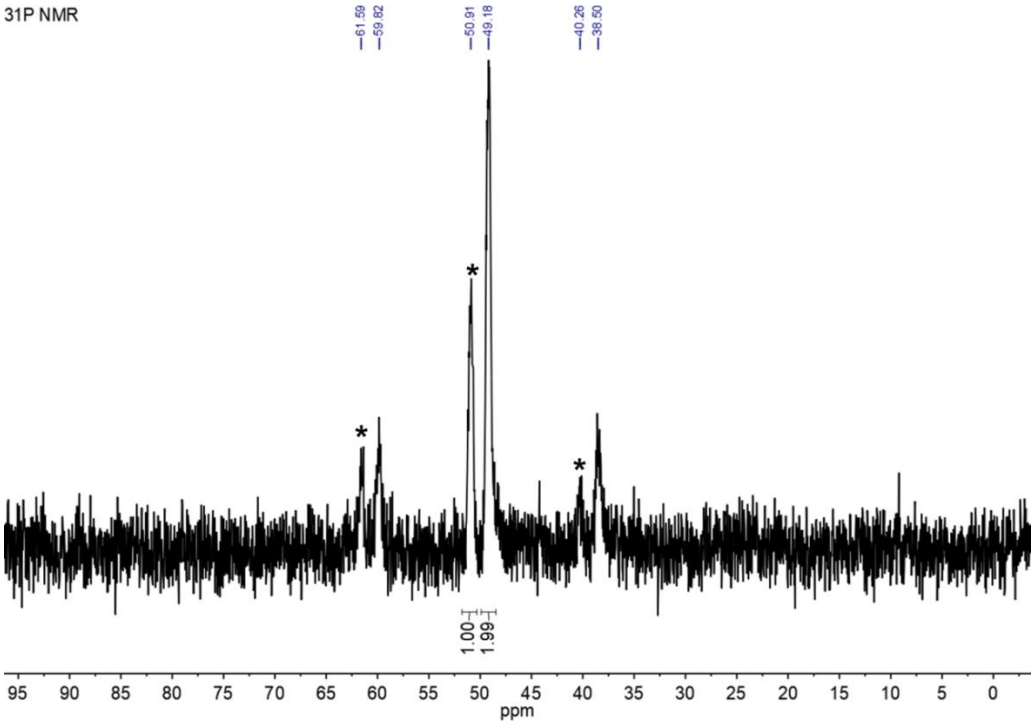

*Diastereomers of **7**.

Re-opening 6 to form [*cis*–Pt$_2$(κ^1:μ:κ^1–NHC,S)(κ^2:μ:κ^2–P,S)][Cl]$_2$ (5)

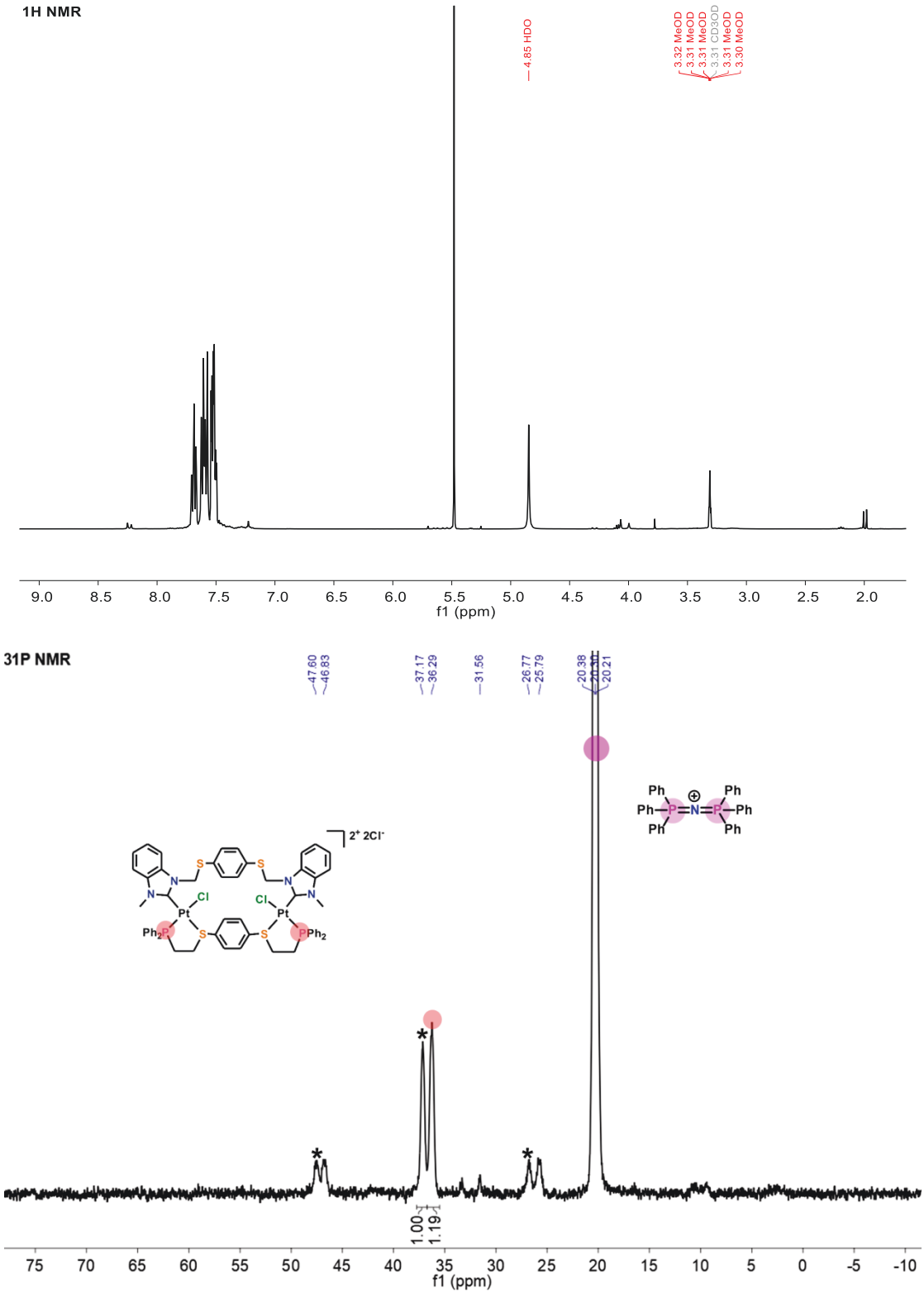

*Diastereomers of **5**.

Re-opening (5) to form [*cis*–$Pt_2Cl_4(\kappa^1{:}\mu{:}\kappa^1$–NHC,S)($\kappa^1{:}\mu{:}\kappa^1$–P,S)] (4a)

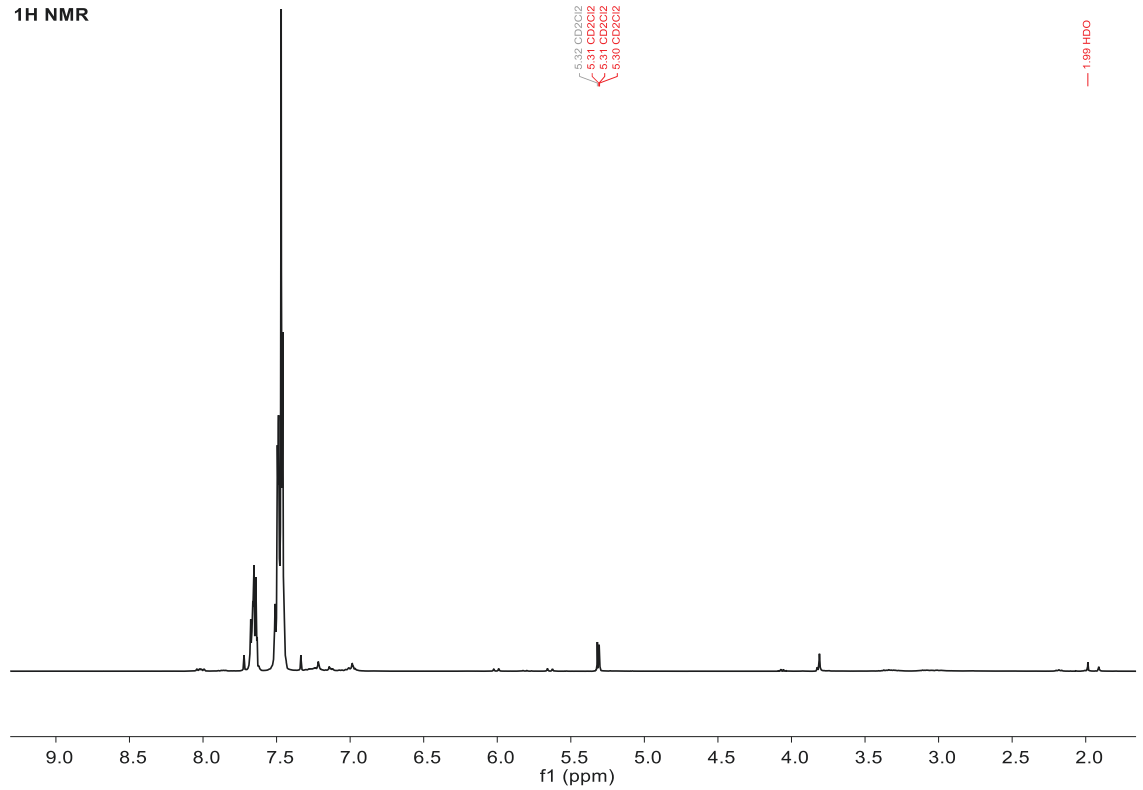

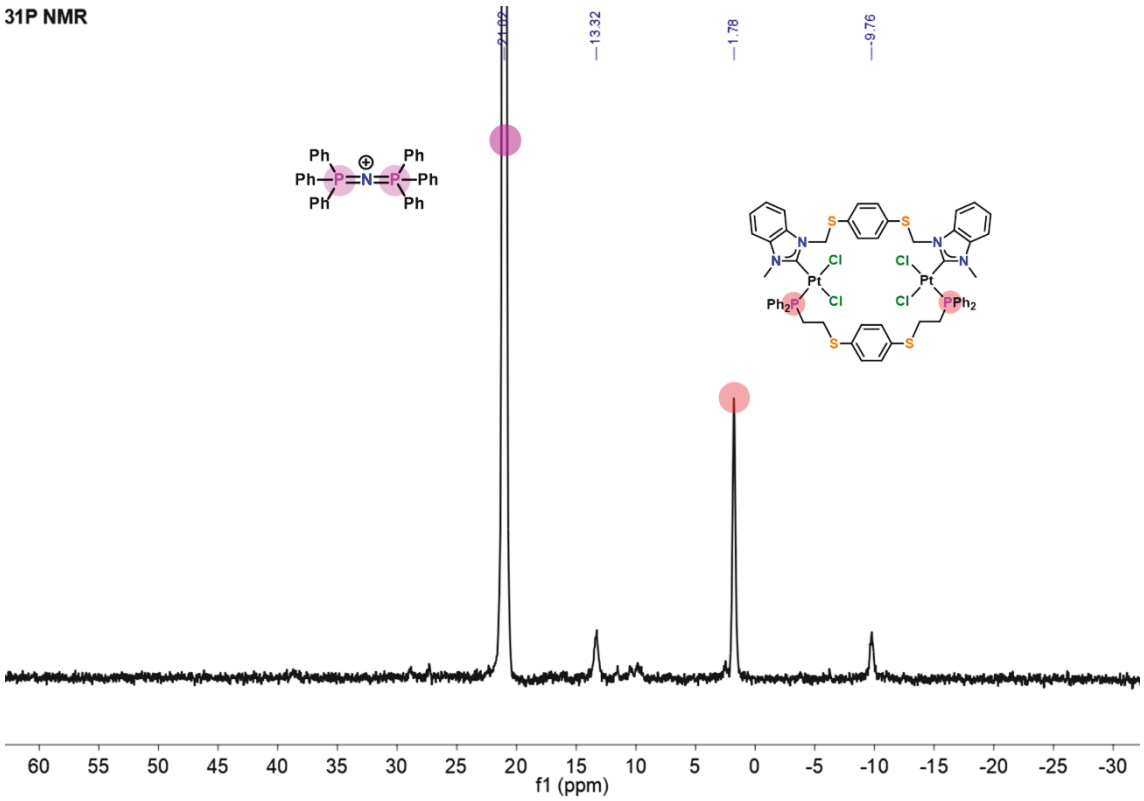

Mass Spectra

MALDI-TOF MS of $[Pt_2Cl_4(\kappa^1{:}\mu{:}\kappa^1\text{–NHC,S})]$ (2)

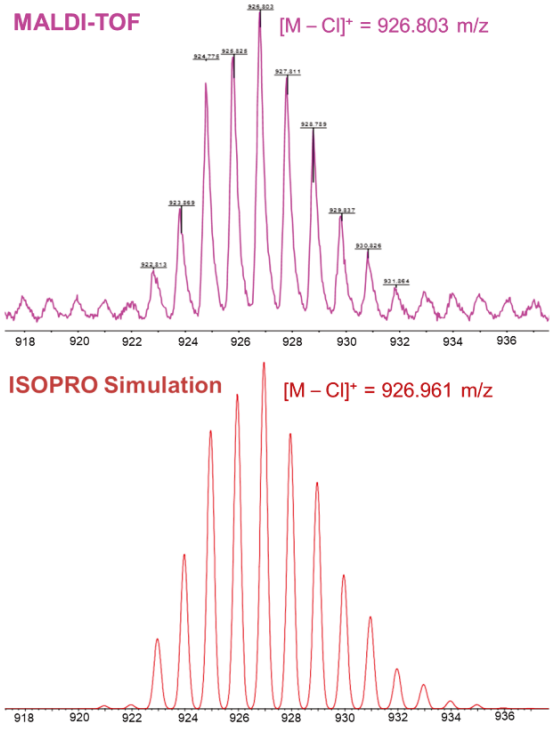

HRMS (ESI+) of Fully Open Macrocycle (4)

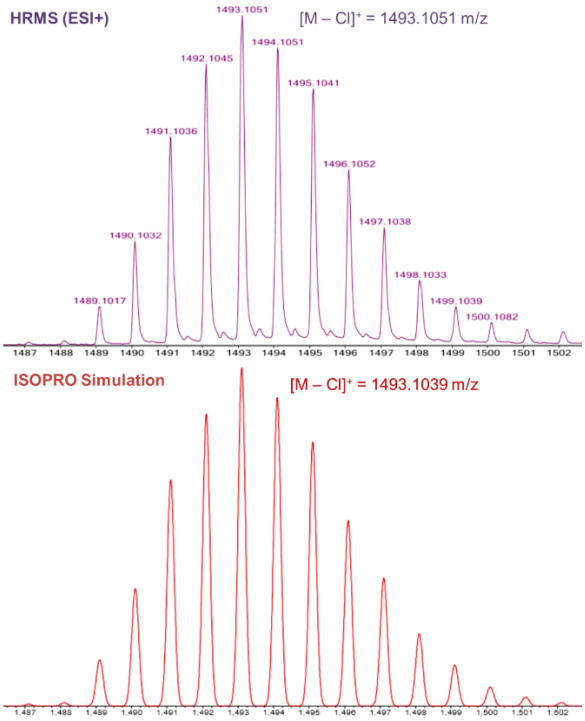

HR-MS (ESI+) of Semi-Open Macrocycle [*cis*–$Pt_2Cl_2(\kappa^1{:}\mu{:}\kappa^1$–NHC,S)($\kappa^2{:}\mu{:}\kappa^2$–P,S)][Cl]$_2$ (5)

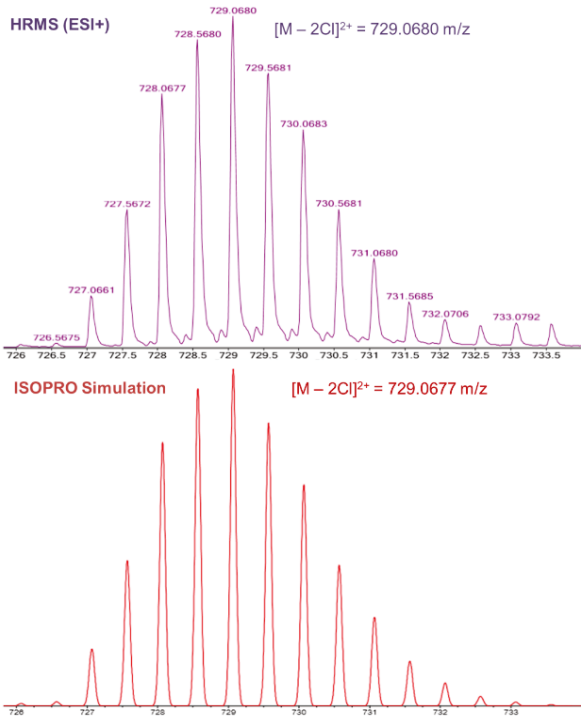

MALDI-TOF MS of Fully Closed/Semi-Open Complex [*cis*–$Pt_2(\kappa^1{:}\mu{:}\kappa^2$–NHC,S)($\kappa^2{:}\mu{:}\kappa^2$–P,S)$CH_3OH$][$BF_4$]$_4$ (6)

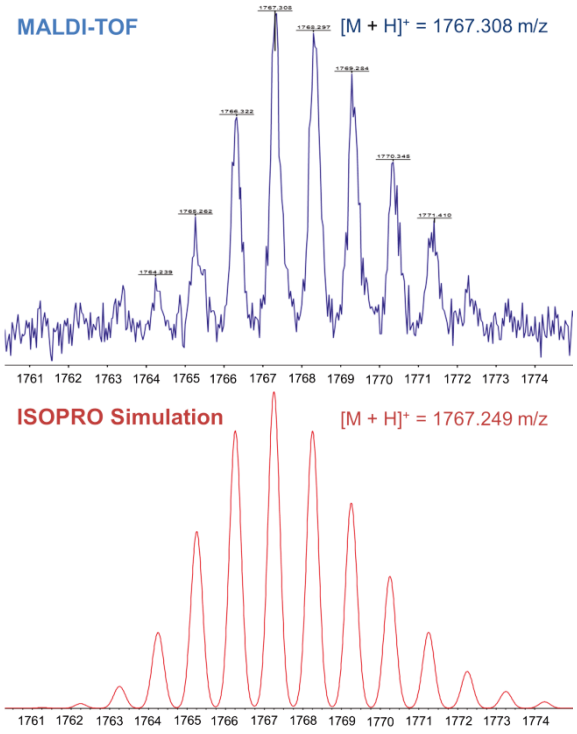

References.

(1) Dolomanov, O. V.; Bourhis, L. J.; Gildea, R. J.; Howard, J. A. K.; Puschmann, H. OLEX2: a complete structure solution, refinement and analysis program. *J. Appl. Crystallogr. 2009*, *42,* 339-341.
(2) Sheldrick, G. M. SHELXT - Integrated space-group and crystal-structure determination. *Acta Crystallogr., Sect. A: Found. Adv. 2015*, *71,* 3-8.
(3) Sheldrick, G. M. Crystal structure refinement with SHELXL. *Acta Crystallogr., Sect. C: Struct. Chem. 2015*, *71,* 3-8.